Gondwana Research 25 (2014) 522–545

Contents lists available at ScienceDirect

Gondwana Research

journal homepage: www.elsevier.com/locate/gr

Contrasting styles of Phanerozoic and Precambrian continental collision

E. Sizova [a,*], T. Gerya [a,b], M. Brown [c]

[a] ETH-Zurich, Institute of Geophysics, Sonnegstrasse 5, 8092 Zurich, Switzerland
[b] Geology Department, Moscow State University, 119199 Moscow, Russia
[c] Department of Geology, University of Maryland, College Park, MD 20742, USA

ARTICLE INFO

Article history:
Received 24 May 2012
Received in revised form 30 November 2012
Accepted 12 December 2012
Available online 7 January 2013

Keywords:
Continental collision
Exhumation
Precambrian orogenesis
Slab breakoff
Tectonics

ABSTRACT

There are differences in the style of collisional orogens between the Phanerozoic and the Precambrian, most notably the appearance of blueschists and ultrahigh pressure metamorphic (UHPM) rocks in the geological record since the late Neoproterozoic, whereas these rocks are absent from older orogens. Understanding collisional orogenesis in the context of present-day values for ambient upper-mantle temperature and radiogenic heat production provides a reference from which to extrapolate back to conditions in the Precambrian. To evaluate differences in the way Phanerozoic and Precambrian collisional orogens develop, a series of experiments was run using a 2-D petrological–thermomechanical numerical model in which the collision of spontaneously moving continental plates was simulated for values of ambient upper-mantle temperature and radiogenic heat production increasing from those appropriate to the present-day. Thus, models of modern collisional orogens involving different modes of exhumation of UHPM rocks were extrapolated back to conditions appropriate for the Precambrian. Based on these experiments an increase of the ambient upper-mantle temperature to >80–100 K above the present-day value leads to two distinct modes of collision that are different from the modern collision regime and for which the terms truncated hot collision regime (strong mafic lower continental crust) and two-sided hot collision regime (weak felsic lower continental crust) are proposed. Some Proterozoic orogens record post-extension thickening to generate counter-clockwise metamorphic *P–T* paths followed by slow close-to-isobaric retrograde cooling, such as occurred in the Paleoproterozoic Khondalite belt in the North China craton and the late Mesoproterozoic–early Neoproterozoic Eastern Ghats province, part of the Eastern Ghats belt of peninsular India. These orogens have similarities with the truncated hot collision regime in the numerical models, assuming subsequent shortening and thickening of the resulting hot lithosphere. Other Proterozoic orogens are characterized by clockwise looping metamorphic *P–T* paths and extensive granite magmatism derived from diverse crustal and subcontinental lithospheric mantle sources. These orogens have similarities with the two-sided hot collision regime in the numerical models. Both regimes are associated with shallow slab breakoff that precludes the formation of UHPM rocks. The temperature of the ambient upper-mantle where this transition in geodynamic regimes occurs corresponds broadly to the Neoproterozoic Era.

1. Introduction

The relevance of studies of modern collisional orogens to understanding collisional orogenesis in the Precambrian is still an enigmatic issue. For this reason it is common to use a uniform approach based on the plate tectonics paradigm to interpret Precambrian geology and continental reconstructions (e.g. Cawood et al., 2006; Condie and Kröner, 2008; de Kock et al., 2009). Indeed, there are many similarities in rock types between modern and Proterozoic orogens, such as the presence of dismembered ophiolite complexes and eclogites (e.g. Moores, 2002; Brown, 2006, 2007, 2008), as well as a number of changes during the late Archean in the style and chemistry of magmatic rocks (e.g. Valley et al., 2005; Smithies et al., 2007; Condie, 2008; Martin et al., 2010; Keller and Schoene, 2012), the rates of addition of juvenile crust vs. crustal reworking (Dhuime et al., 2012), and the sites of continental growth (Condie and Kröner, 2013) that are consistent with a global plate tectonics regime during the Proterozoic and, perhaps, during the Neoarchean. In addition, seismic reflection and refraction surveys have determined the internal architecture of the continents (e.g. Korja and Heikkinen, 2005; Hammer et al., 2010) and identified dipping structures that displace the Moho (e.g. Calvert et al., 1995; Oueity and Clowes, 2010) back to the Neoarchean, features that are consistent with terrane accretion and collisional orogenesis.

These geological, geochemical and geophysical data from Neoarchean and Proterozoic provinces require the elimination of ocean basins by subduction of oceanic lithosphere, consistent with the large lateral displacement of cratons that are recognized based on paleomagnetic data (e.g. Evans and Mitchell, 2011), which has led many researches to the conclusion that a plate tectonics regime similar to that on modern Earth operated in the Precambrian, perhaps from as early as the late Mesoarchean (e.g. Condie and Pease, 2008; Condie and O'Neill, 2010;

* Corresponding author. Tel.: +41 44 633 66 23.
E-mail address: sizovaev@gmail.com (E. Sizova).

1342-937X/$ – see front matter © 2013 International Association for Gondwana Research. Published by Elsevier B.V. All rights reserved.
http://dx.doi.org/10.1016/j.gr.2012.12.011

Gerya, 2014). However, there are no examples of blueschists or evidence of the deep subduction of continental crust in the form of exhumed ultrahigh pressure metamorphic rocks in the geological record before the Neoproterozoic (e.g. Brown, 2006, 2007). Since these features are characteristic of the Phanerozoic style of plate tectonics and collisional orogenesis, some researchers have concluded that the modern plate tectonics regime began only during the Proterozoic (e.g. Hamilton, 1998), possibly as late as the Neoproterozoic (e.g. Stern, 2005; Hamilton, 2011). Thus, a purely uniformitarian approach to collisional orogenesis in the Precambrian may be inappropriate. Indeed, there is a growing body of research pointing to a distinct style of deformation and metamorphism in Neoarchean and Paleoproterozoic orogens (e.g. Choukroune et al., 1995; Rey et al., 2003; Cagnard et al., 2006; Rey and Houseman, 2006; Cagnard et al., 2007; Chardon et al., 2009; Cagnard et al., 2011).

It is only recently that parameterized numerical modeling and analog experiments have been used to investigate the stabilization of cratons and major transitions in tectonic regime with secular evolution on Earth (e.g. Rey and Houseman, 2006; Burov and Yamato, 2008; van Hunen and van den Berg, 2008; Gapais et al., 2009; Gray and Pysklywec, 2010; Rey and Coltice, 2010; Sizova et al., 2010; Moyen and van Hunen, 2011; van Hunen and Allen, 2011; Maierova et al., 2014; Vogt and Gerya, 2014). These studies support a mobile lid regime based on lateral displacement of lithospheric plates and elimination of ocean basins by subduction since the Mesoarchean–Neoarchean (e.g. van Hunen and van den Berg, 2008; Sizova et al., 2010; Moyen and van Hunen, 2011). To resolve some of the issues related to the first appearance of blueschists and ultrahigh pressure metamorphic rocks in the geological record during the Neoproterozoic (e.g., Stern, 2005; Brown, 2006, 2007), we have undertaken a systematic investigation of the effects of a warmer ambient upper-mantle, higher crustal radiogenic heat production, changes in thickness and chemical buoyancy of the continental lithosphere, and differences in lower crustal composition and rheology on the style of collisional orogenesis. In particular, we are interested in what conditions earlier in Earth history prevented blueschists and UHPM rocks from developing on Earth prior to the Neoproterozoic.

1.1. Phanerozoic vs. Precambrian orogens

Phanerozoic collisional orogenic systems generally produce characteristic clockwise metamorphic pressure–temperature (*P*–*T*) paths (e.g. Brown, 1993, 2001) and may generate extreme ultrahigh-pressure metamorphism (UHPM) of subducted continental crust (Ernst, 2001; Liou et al., 2004), which may melt during exhumation (Auzanneau et al., 2006), or if subducted past the “point of no return” may be transported into the deep mantle (e.g., Irifune et al., 1994; Domanik and Holloway, 2000; Searle et al., 2001; Dobrzhinetskaya and Green, 2005; Liu et al., 2007; Wu et al., 2009; Faryad et al., 2013). Continental rocks are subjected to ultrahigh-pressure metamorphism (UHPM) at temperatures from ~700 to 950 °C and pressures >2.8 up to 6.0 GPa, corresponding to depths of ~100 to >200 km (e.g. Liou et al., 2004). These UHPM units are subsequently exhumed to middle crustal depths while erosion or younger tectonic events are responsible for final exhumation to the surface.

More than twenty UHPM terranes have been documented all over the world; with two exceptions at 660–655 Ma (John et al., 2004) and 620 Ma (Jahn et al., 2001), all of them are of Phanerozoic age (Brown, 2007). They lie within major continental collision belts and extend for several hundred kilometers along strike; most are in Eurasia, with rare examples in Africa, Central America and Antarctica. Many of the exhumed UHPM rocks exposed at the surface occur as subhorizontal sheets 1–5 km in thickness, bounded by normal faults on the top and reverse faults on the bottom, sandwiched between high-pressure or lower-grade metamorphic units (Kaneko et al., 2000; Ernst, 2001; Liou et al., 2004). Typically, the UHPM rocks now form the cores of antiformal nappe stacks that define structural domes 5–50 km across (Faure et al., 2003; Xu et al., 2006; Epard and Steck, 2008). The upper levels of many HPM–UHPM terranes are dominated by extensional structures formed during and/or after initial exhumation from UHPM conditions (Andersen and Jamtveit, 1990; Ratschbacher et al., 2000; Avigad et al., 2003).

As discussed above, the appearance of UHPM complexes in the geological record during the Neoproterozoic raises an important question about a different style of orogenesis earlier in Earth history. It is widely accepted that the Earth has been cooling since its formation due to the decline in radiogenic heat production (e.g. Abbott et al., 1994; Labrosse and Jaupart, 2007), although the process may not have been monotonic (e.g. Sleep, 2007). The greater rate of production of continental crust prior to 3.0 Ga (Dhuime et al., 2012) and the occurrence of tonalites–trondhjemites–granodiorites and komatiites, which are largely restricted to the Archean (Goodwin, 1991), are consistent with a hotter Earth. Ambient mantle potential temperatures are inferred to have been significantly higher than the present day, which would have led to the production of a greater volume of primary melts with higher MgO (McKenzie and Bickle, 1988; Nisbet et al., 1993; Herzberg et al., 2007, 2010).

Although there is no debate about a hotter ambient upper-mantle in the past, there is considerable uncertainty in the estimate of how much hotter it might have been. Based on Labrosse and Jaupart (2007) and Herzberg et al. (2010), the ambient upper-mantle temperature from the Paleoarchean to the Paleoproterozoic might have been 250–150 K higher than the present day. Even at 1.0 Ga the ambient upper-mantle temperature was probably ~100 K warmer than at present, and it was probably ~60 K warmer at the dawn of the Phanerozoic. However, field observations of the Archean sediment record and experimental determination of phase relations in hydrous komatiitic melts have shown that the upper mantle liquidus temperatures could not have been much hotter than today (<100 °C; Galer, 1991; Campbell and Griffiths, 1992; Grove et al., 1994; Parman et al., 1997). Higher ambient upper-mantle temperatures are likely to affect the rheology and tectonics of the lithosphere (e.g. Davies, 1992; de Wit, 1998; Burov and Yamato, 2008; van Hunen and van den Berg, 2008; Sizova et al., 2010).

Archean and Paleoproterozoic orogens in particular commonly comprise large areas of monotonous high-temperature, low-to-moderate pressure metamorphic rocks with extensive magmatism that has contributed significantly to crustal growth (e.g. Brown, 2007; Ahäll and Connelly, 2008; Gapais et al., 2009; Kukkonen and Lauri, 2009; Smithies et al., 2011; Dhuime et al., 2012; Percival et al., 2012). These orogens formed above warmer mantle than modern orogens, and remained hot and mechanically extremely weak during deformation over protracted periods of time; Chardon et al. (2009) referred to these as ultra-hot orogens. Rey and Houseman (2006) and Gapais et al. (2009) argued that convergence involving warm and rather weak, buoyant lithosphere in the Precambrian would result in more homogeneous lithospheric deformation that would be reflected in the distributed patterns of strain, lower topographic relief and lower exhumation rates characteristic of these orogens. Even at the end of the Proterozoic Era, granulite and ultrahigh temperature metamorphism occurs in most of the orogenic belts that suture the cratonic elements of Gondwana (Cawood and Buchan, 2007).

Brun (2002) proposed that the fundamental difference between ultra-hot orogens and cold orogens is the Moho temperature, which determines the strength of the upper mantle, and Burov and Yamato (2008) used numerical experiments to investigate the importance of Moho temperature in controlling the style of collisional orogenesis. Burov and Yamato (2008) identified that continental subduction is possible only in the case of strong mantle lithosphere characterized by Moho temperatures below T_m<500 °C; thus, the formation and exhumation of UHPM rocks can only occur in this regime. Increasing Moho temperature leads to lithospheric folding at 500 °C<T_m<650 °C or pure shear thickening at 550 °C<T_m<650 °C, and finally to Rayleigh–Taylor instabilities at T_m>650 °C. Subsequently, Gray and Pysklywec (2010) used numerical experiments to investigate the behavior of continental lithosphere during Neoarchean collision taking into account the initial elevated geotherm, higher radiogenic heat production and different densities of lithospheric and sub-lithospheric mantle at that time. These authors proposed three dominant styles of Neoarchean mantle lithosphere deformation during collision: pure-shear thickening; imbrication (the strong upper portion of the mantle lithosphere underthrusts adjacent mantle lithosphere along a weak/decoupling crust–mantle interface); and, underplating.

The pattern of crustal metamorphism in the geological record indicates secular change and records two major discontinuous transitions in the thermal structure of orogenic systems that separate three geodynamic regimes in the evolution of Earth (Brown, 2006, 2007). The first transition is identified by the appearance of eclogite–high-pressure granulite metamorphism (E–HPM) and ultrahigh-temperature metamorphism (UHTM) in the geological record across the Archean–Proterozoic boundary; this style of metamorphism is dominant from the Neoarchean to the Cambrian. The second transition is identified by the appearance of blueschists and UHPM rocks in the Neoproterozoic Era, demanding deep subduction of the continental crust and its return to crustal depths; blueschists and UHPM rocks are characteristic of Phanerozoic collisional orogens (Brown, 2006, 2007).

The first discontinuous transition was investigated by Sizova et al. (2010) in a series of experiments using a numerical model of ocean–continent convergence and ocean plate subduction, and covering a wide range of parameter space. These authors showed that the appearance of E–HPM and UHTM during the Mesoarchean–Neoarchean related to a change in the geodynamic regime as one-sided subduction became possible. The systematic investigation of the second transition with a series of experiments using a numerical model of ocean plate subduction and continent–continent collision is the main goal of the present paper.

The results reported here complement the study by van Hunen and Allen (2011) who used 3-D fully dynamical models to investigate the self-consistent dynamics of slab breakoff after continental collision. They proposed that in a continental collisional setting a weak oceanic plate, which is considered typical for the Precambrian, would have led to earlier and shallower break-off of the oceanic plate than happens during collision today, when slabs are stronger. As a result, continental crust cannot be taken down to the depth required to form blueschists and UHPM rocks, and these rocks would not be expected to be present in the Precambrian geological record.

Using a numerical model of collision driven by spontaneously moving plates, Sizova et al. (2012) investigated a variety of exhumation mechanisms for HPM–UHPM rocks, including vertical crustal extrusion, large-scale crustal stacking and trans-lithospheric diapirism. These authors demonstrated the importance of a non-prescribed convergence velocity condition and the effect of fluid- and melt-related weakening in enabling and controlling the exhumation mechanisms during continental collision. To investigate possible changes in the style of collision earlier in Earth history that could have prevented UHPM rocks from developing, a series of numerical experiments was designed based on different exhumation mechanisms for UHPM rocks investigated in the earlier study by Sizova et al. (2012). These experiments systematically investigate increases (compared to present day values) in ambient upper-mantle temperature, crustal radiogenic heat production, and thickness and chemical buoyancy of the continental lithosphere, as well as the effects of lower crustal composition and rheology for identified transitions between modern and Precambrian collision styles. The point of the modeling is not to predict the evolution of any particular orogen, but to understand the controlling factors that determine differences in style of orogenesis.

2. Numerical model description

2.1. Numerical model design

The 2D petrological–thermomechanical numerical model used in this work simulates the processes of oceanic subduction followed by continental collision in a 4000 km wide × 1400 km deep lithosphere–asthenosphere section. The model is based on the I2VIS code (Gerya and Yuen, 2003) using conservative finite differences and a non-diffusive marker-in-cell technique to simulate multiphase flow. A 40 Ma old oceanic plate with a width of 400/600 km is located between two continental plates; the oceanic plate is part of the left-hand composite oceanic–continental plate (Fig. 1). The right-hand continental plate is 1700 km wide and fixed whereas the left-hand continental plate is 1660/1860 km wide (attached to an oceanic plate 600/400 km wide, respectively) and it is initially pushed to the right with a constant velocity of 5 cm/yr, imposed in a small domain in the continental lithosphere at the left edge of the model. The push is maintained for the first 6/10 million years of model evolution (according to the length of the oceanic plate, which is 400/600 km, respectively) until the left-hand continent reaches the right-hand continent after which the push is discontinued and subduction is driven spontaneously by slab pull. Thus, the collision stage in the model evolves self-consistently according to a spontaneous plate convergence velocity regulated by the slab pull, asthenospheric viscosity and buoyancy of the subducting continental crust. The models use a grid resolution of 1361 × 351 nodes with variable grid spacing. This allows a highest grid resolution of 1 × 1 km in the area of interest covering 1050 km horizontally (from x = 1900 to 2950 km) and 250 km vertically (from z = 0 to 250 km). The number of Lagrangian markers is around 13 million.

On the left, the oceanic lithosphere is generally attached abruptly to the continental lithosphere, although in some experiments the attachment is more gradual, with sedimentary rocks overlying a narrow or wide passive margin (50/150 km wide), whereas on the right a prism of sedimentary rocks is set against the continent above a right-dipping weak zone along the left edge of the right-hand continental plate (Fig. 1). The cooling age of the oceanic lithosphere is 40 Ma. The oceanic crust is represented by 2 km of hydrothermally altered basalts underlain by 5 km of gabbroic rocks. The upper continental crust is felsic (thickness is 20 km with a weaker rheology of wet quartzite, Table 1) whereas the lower continental crust is generally mafic (thickness is 20 km with a stronger rheology of plagioclase An_{75}, Table 1), although in some experiments the lower crust is felsic (thickness is 20 km with a weaker rheology of wet quartzite, Table 1). At the onset of subduction, both the lithospheric mantle and the asthenosphere consist of anhydrous peridotite. During the process of subduction, the mantle overlying the subducting slab becomes hydrated as a result of migration of fluid liberated by metamorphic reactions in the slab. The stable fluid content for each lithology was obtained using free energy minimization (Connolly, 2005). The flow law for each lithology and other physical parameters for the experiments are presented in Table 1.

Subduction of the oceanic plate is initiated by prescribing a weak zone in the mantle with the rheology of wet olivine (Ranalli, 1995) and low plastic strength (internal friction coefficient of 0.1) between the oceanic plate and the right-hand continental plate (e.g. Toth and Gurnis, 1998). The weak zone extends from the bottom of the continental crust to the bottom of the continental lithosphere (140 km for present-day conditions). The chemical density contrast between the subcontinental lithospheric mantle and the underlying mantle is 20 kg/m^3 for present-day conditions (Djomani et al., 2001).

All mechanical boundary conditions are free-slip. The top surface of the lithosphere is treated as an internal free surface by using an 18–20 km thick top layer with low viscosity (10^{18} Pa s) and density (1 kg/m^3 for air and 1000 kg/m^3 for sea water below the z = 10 km level). The large viscosity contrast caused by these low viscosity boundary layers minimizes shear stresses ($<10^4$ Pa) at the top of the lithosphere making it an efficient free surface (cf. Schmeling et al., 2008). This upper boundary evolves by erosion and sedimentation (see Supplementary materials for details).

The initial temperature field for the oceanic plate is derived from the oceanic geotherm computed for the given cooling age and the

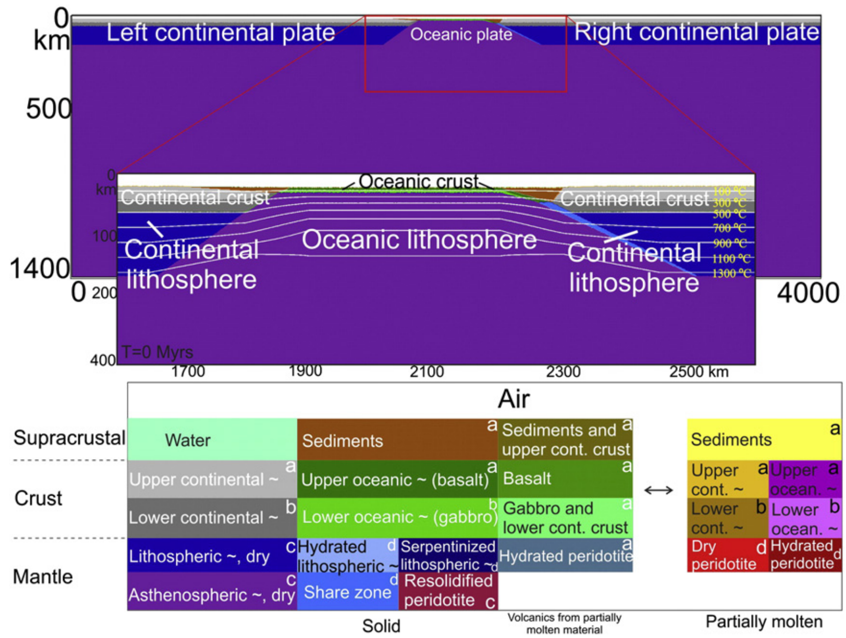

Fig. 1. Initial configuration of the numerical model (see text and Sizova et al. (2010) for details). White lines are isotherms shown for increments of 200 °C starting from 100 °C. Colors indicate materials (e.g. rock type or melt) which appear in subsequent figures. Letters in blocks show the rheology that is used for the materials (see Table 1): a — wet quartzite; b — plagioclase An75; c — dry olivine; and d — wet olivine. The resolution of the model at x = 1900–2950 km and y = 0–250 km is 1 × 1 km, in the remaining part of the model resolution gradually changes to up to 10 × 10 km.

temperature of the asthenospheric upper mantle (Turcotte and Schubert, 2002). In the continental lithosphere, the initial thermal structure is determined based on the radiogenic heat production of the upper and lower crust, where the surface temperature (0 °C) and the upper-mantle temperature at the bottom of the lithosphere (for 140 km-thick lithosphere, 1344 °C; for 160 km, 1357 °C) are prescribed. The initial temperature gradient in the underlying mantle is 0.5 °C/km. During the numerical experiments this initial thermal structure evolves spontaneously.

Because the H_2O transport model does not permit complete hydration of the peridotitic mantle, the mantle solidus is intermediate between the wet and dry peridotite solidi. In reality, variable hydration would permit melting over a range of temperatures and water contents (e.g. Grove et al., 2006). To account for this behavior we assume that the degree of both hydrous and dry melting is a linear function of pressure and temperature (e.g. Gerya and Yuen, 2003). In this model the volumetric degree of melting M_0 is,

$$M_o = \begin{cases} 0 & T < T_{\text{solidus}} \\ \dfrac{T - T_{\text{solidus}}}{T_{\text{liquidus}} - T_{\text{solidus}}} & T_{\text{solidus}} < T < T_{\text{liquidus}} \,, \\ 1 & T > T_{\text{liquidus}} \end{cases} \tag{1}$$

where T_{solidus} and T_{liquidus} are, respectively, solidus temperature (wet and dry solidi are used for the hydrated and dry mantle, respectively) and dry liquidus temperature at a given pressure and rock composition (see Table 1). To simulate melt extraction from partially molten rocks (e.g. Nikolaeva et al., 2008; Gerya and Meilick, 2011) we define a melt extraction threshold M_{max} and a non-extractable amount of melt $M_{\text{min}} < M_{\text{max}}$ that will remain in the source. The influence of these parameters on subduction dynamics and crustal growth is investigated for the case of constant $M_{\text{max}}/M_{\text{min}} = 2$.

Markers track the amount of melt extracted during the evolution of each experiment. The total amount of melt, M, for every marker takes into account the amount of previously extracted melt and is calculated as,

$$M = M_0 - \sum_n M_{\text{ext}}, \tag{2}$$

where $\sum_n M_{\text{ext}}$ is the total melt fraction extracted during the previous n extraction episodes. Once the total amount of melt, M, computed from Eqs. (1) and (2) for a given marker, exceeds M_{max}, the extractable melt fraction $M_{\text{ext}} = M - M_{\text{min}}$ is assumed to migrate upward and the value of $\sum_n M_{\text{ext}}$ is updated. We assume that melt migration is rapid compared to the deformation of unmelted mantle, so that the velocity of the melt is independent of mantle dynamics (Elliott et al., 1997; Hawkesworth et al., 1997). Thus, the extracted melt is transported instantaneously to the surface forming new volcanic crust above the extraction area.

The weakening effects of ascending fluids and melts are included in the model (Sizova et al., 2010; Gerya and Meilick, 2011). During aqueous fluid propagation from the slab the yield strength, σ_{yield}, of the percolated rocks is decreased according to $\lambda_{\text{fluid}} = 1 - P_{\text{fluid}}/P_{\text{solid}}$ (see the Supplementary materials). Similarly, during a melt extraction episode, the yield strength, σ_{yield}, of rock in the column between the source of the melt and the surface, is decreased according to $\lambda_{\text{melt}} = 1 - P_{\text{melt}}/P_{\text{solid}}$. A low value of $\lambda_{\text{fluid}} = \lambda_{\text{melt}} = 0.001$ was used in the numerical experiments providing significant weakening of rocks subjected to free fluid/melt propagation and creating favorable conditions for realistic modern-style subduction (Sizova et al., 2010).

The compressibility of the subducting oceanic crust was increased by a factor of two relative to other rocks. This allowed simulation to a first order of the effects of an increased slab pull related to the eclogitization reaction in the subducting slab (e.g. Mishin et al., 2008; Baumann et al., 2010). A more detailed description of the model and the numerical techniques employed in this study are given in the Supplementary materials and in Sizova et al. (2010).

2.2. Modeling procedure

To investigate possible differences in the formation of Phanerozoic and Precambrian collision belts, four series of experiments were undertaken, extrapolating back from reference models that yielded different exhumation mechanisms of UHPM rocks (Sizova et al., 2012), since this is the most distinctive feature of the modern collisional

Table 1

Properties of the materials used in the experiments (Bittner and Schmeling, 1995; Clauser and Huenges, 1995; Ranalli, 1995; Schmidt and Poli, 1998; Turcotte and Schubert, 2002; Burg and Gerya, 2005). ρ_0—density, k—thermal conductivity, $T_{solidus,\ liquidus}$—solidus and liquidus temperatures of the crust, H_r, H_L—heat production (radiogenic, latent), E—activation energy, n—stress component, A_D—material constant, V—activation volume, and sin(φdry)—effective friction coefficient for dry rocks.

Material[a]	ρ_0 [kg/m^3] (solid)	k [W/(m∗K)]	Rheology/ flow law	$T_{solidus}$ [K]	$T_{liquidus}$ [K]	H_r [μW/m^3]	H_L [kJ/kg]	E [kJ/ mol]	n	A_D [Mpa^{-II}∗ s^{-1}]	V [J/ (MPa∗ mol)]	Cohesion [MPa]	sin (φdry)
Sedimentary and felsic crust	Sediments:2600 Felsic crust: 2700	$\left[0.64+\frac{807}{(T+77)}\right]\times\exp(0.00004\cdot P_{MPa})$	Wet quartzite	At $P<1$ $889+\frac{17900}{(P+54)}+\frac{20200}{(P+54)^2}$ at $P>1200$ MPa $831+0.06\cdot P$	$1262+0.009\cdot P$	2 felsic crust:1	300	154	2.3	$10^{-3.5}$	0	10	0.15
Melt-bearing sediments and felsic crust	2400	–//–	–//–	–//–	–//–	–//–	–//–	0	1	–//–	–//–	1	0
Basalts	3000	$\left[1.18+\frac{474}{(T+77)}\right]\times\exp(0.00004\cdot P_{MPa})$	Wet quartzite	at $P<1600$ MPa $973-\frac{70400}{(P+354)}+\frac{77800000}{(P+354)^2}$ at $P>1600$ MPa $935+0.0035\cdot P+0.0000062\cdot P^2$	$1423+0.105\cdot P$	0.25	380	154	2.3	$10^{-3.5}$	0	10	0.1
Melt-bearing basalts	2900	–//–	–//–	–//–	–//–	–//–	–//–	0	1	–//–	–//–	1	0
Gabbroic/mafic crust	3000	$\left[1.18+\frac{474}{(T+77)}\right]\times\exp(0.00004\cdot P_{MPa})$	Plagioclase An_{75}	–//–	$1423+0.105\cdot P$	0.25	380	238	3.2	$10^{-3.5}$	0	10	0.6
Melt-bearing gabbroic/ mafic crust	2900	–//–	Wet quartzite	–//–	–//–	–//–	–//–	0	1	–//–	–//–	1	0
Lithosphere–asthenosphere mantle	3300	$\left[0.73+\frac{1293}{(T=77)}\right]\times\exp(0.00004\cdot P_{MPa})$	Dry olivine	$1394+0.133\cdot P_{MPa}-0.0000051\cdot P^2{}_{MPa}$	$2073+0.114\cdot P$	0.022	–	532	3.5	$10^{4.4}$	8	10	0.6
Hydrated mantle/ hydrated mantle in subduction zone/ serpentinized mantle	3200 (hydrated) 3000 (serpentinized) 3300 (shear zone)	–//–	Wet olivine	Hydrated mantle : at $P<1600$ MPa : $973+\frac{70400}{(P+354)}+\frac{77800000}{(P+354)^2}$ at $P>1600$ MPa : $935+0.0035\cdot P+0.0000062\cdot P^2$	Hydrated mantle : $2073+0.114\cdot P$	0.022	Hydrated mantle: 300	470	4	$10^{3.3}$	–//–	10	0.1
Dry/wet melt-bearing mantle	3300/2900	–//–	Dry/wet olivine	–//–	–//–	–//–	–	0	1	$10^{4.4}$	–//–	1	0
Reference[b]	1, 2	3	4	5	5	1	1, 2	4	4	4	4, 1		

[a] For all types of rocks: $C_p = 1000$ J/kg, $\alpha = 3*10^{-5}$ K^{-1} and $\beta = 1*10^{-3}$ MPa^{-1}.

[b] 1 = Turcotte and Schubert (2002), 2 = (Bittner and Schmeling (1995), 3 = Clauser and Huenges (1995), 4 = Ranalli (1995), and 5 = Schmidt and Poli (1998).

orogenesis with stiff converging lithospheres. The modeling is restricted to an investigation of variations in the most likely first order parameters controlling collisional orogenesis when extrapolating back to the Precambrian (ambient upper-mantle temperature, crustal radiogenic heat production, and thickness and chemical buoyancy of the continental lithosphere).

The distinct modes of exhumation of UHPM rocks associated with different collision scenarios from Sizova et al. (2012) are: large-scale crustal stacking (reference model CS), trans-lithospheric diapirism (reference model TD) and vertical crustal extrusion (reference model VE); in addition, shallow crustal delamination (reference model SD) occurs when the lower crust is felsic. All experiments relating to present-day conditions involve continental collision of spontaneously moving plates, subduction of the continental lithosphere, oceanic slab detachment and exhumation of UHPM rocks.

To extrapolate the reference models back in time, the four first-order parameters listed above that have gradually decreased throughout Earth history (e.g. Abbott et al., 1994; Djomani et al., 2001; Chacko, 2003; Korenaga, 2006) were progressively increased. Thus, in the numerical experiments, the upper-mantle temperature was increased in a series of steps up to 150 K higher than the present-day value ($\Delta T = 150$ K)), together with crustal radiogenic heat production (up to 1.5 times higher ($H_r = 1.5 * H_r^0$)), thickness of the continental lithosphere (from 140 km to 160 km (Lt = 140–160 km; Djomani et al., 2001)) and the chemical density contrast between the subcontinental lithospheric mantle and the underlying asthenospheric mantle (where a difference with the underlying mantle of D = 20 kg/m^3 corresponds to the present-day conditions, and D = 50 kg/m^3 corresponds to Proterozoic (Djomani et al., 2001)).

3. Experimental results for models with strong mafic lower crust

3.1. CS model: large-scale crustal stacking

3.1.1. Reference model for present-day conditions

Fig. 2 (and Fig. S1 in Supplementary materials) illustrates the evolution of an experiment with the oceanic lithosphere component of the left-hand plate 600 km long and the width of the incoming passive margin 50 km wide (abrupt passive margin). This geodynamic model was initially run for present-day conditions (Sizova et al., 2012), where the upper-mantle temperature at the bottom of the continental lithosphere at 140 km depth is 1344 °C and the density contrast between the subcontinental lithospheric mantle and the underlying asthenospheric upper mantle is 20 kg/m^3.

As the ocean basin closes at around 10–11 Ma (Fig. 2a) the incoming continental passive margin begins to subduct. At this point the initially imposed push of the left continental plate to the right was deactivated and continental subduction is driven spontaneously by slab pull. The continental plate continues to subduct in a coherent manner to a maximum depth of ~200 km within 6 Ma after the initiation of collision (Fig. 2b). Buoyancy of the deeply-subducted continental crust creates large deviatoric stresses inside the continent, which triggers brittle/plastic failure along the cold Moho boundary within the subducted plate (Fig. 2b). A large coherent crustal-scale block of continental crust separates from the subducting plate and is thrust back over it along a major shear zone producing extremely rapid (within 0.2–0.3 Ma) exhumation of UHPM rocks (Fig. 2c). Strong shear heating results in localized melting of the continental crust lubricating motion along this segment of the shear zone. The continental lithosphere continues to subduct leading to a second large-scale crustal stacking event ca. 0.5 Ma after the first (Fig. 2d).

During ascent of the second block of continental crust subduction is terminated by slab breakoff, which localizes in the continental part of the slab at a depth of ~300 km (Figs. 2d and S1c in Supplementary materials). The breakoff exerts an instantaneous influence on the system resulting in a period of relaxation of the overriding continental plate, which causes a further increase in the elevation of the orogen. After two thousand years slab rollback resumes and drives extension of the orogen.

The subducted continental crust and associated sedimentary rocks rapidly reach a maximum depth of 200 km and then return to middle-to-lower crustal depths in less than 1 Ma. The metamorphic *P–T* conditions for the subducted materials through time were traced using markers (Lagrangian particles; Fig. 2a′, b′, c′, d′). All markers were initially placed in the left-hand continental margin, with two markers (yellow and pink) in the sedimentary rocks and six markers (lilac, dark green, green, blue, dark blue and red) in the upper continental crust (Fig. 2a). The marker locations in the sedimentary rocks spend a longer time in contact with the hot asthenosphere of the mantle wedge than those in the continental crust and consequently they define open *P–T–t* loops with maximum temperatures of ~750 °C at UHPM conditions (Fig. 2a′–d′). In contrast, the marker locations in the upper continental crust (i.e., in the interior of the coherently moving crustal blocks) define very tight *P–T–t* loops, in some cases reaching UHPM conditions but at extremely low temperatures (<400 °C) because of the very rapid subduction and exhumation rates associated with the large-scale crustal stacking. Consequently there is insufficient time for conductive heating of the exhuming thrust blocks of continental crust by contact with the hot asthenosphere of the mantle wedge to raise the temperature significantly (see the two blue markers in Fig. 2c′). As a result, partial melting is localized rather than widespread and melt-induced buoyancy only contributes to the exhumation of the UHPM sedimentary rocks (yellow and pink markers in Fig. 2d′).

Another distinct consequence of this modern collision scenario is delamination of deeply subducted continental mantle lithosphere from the crust—a process that is common during the evolution of modern collisional orogens (e.g. Faccenda et al., 2008; Duretz et al., 2011; Gray and Pysklywec, 2012). Overall, the reference model CS shows rapid exhumation of continental blocks; both the continental crust and the sedimentary rocks record HPM–UHPM *P–T* conditions. The orogen reaches a relatively high elevation.

3.1.2. Extrapolation of the CS model back in time

Modification of the initial parameters (upper-mantle temperature, crustal radiogenic heat production, thickness of the continental lithosphere and the chemical density contrast between the subcontinental lithospheric mantle and the underlying mantle) to extrapolate the CS model back in time leads to notable changes in the internal evolution and geometry of the continental collision (Figs. 3 and S2 in Supplementary materials). Increasing the upper-mantle temperature to 40 K above the present value precludes decoupling of the continental crust and the formation of thrust blocks as occurred in the reference model, although the early evolution of the model is similar with subduction of the oceanic lithosphere and formation of a small back-arc basin. The incoming continental margin is subducted to a depth of ~190 km before subduction is terminated by slab breakoff, which localizes at the oceanic lithosphere–continental lithosphere transition. Slab breakoff results in a period of relaxation of the overriding continental plate. The ascending upper continental crust and associated sedimentary rocks experience decompression partial melting and form a dome structure at crustal depths (Fig. 3b).

The sedimentary rocks (represented by blue and green markers) and continental crust (represented by light blue, pink and red markers) that were subducted to depths up to ~190 km before returning to the upper crust, record HPM–UHPM peak *P–T* conditions and post-peak decompression *P–T–t* paths (Fig. 3b′). As in the reference model, the sedimentary rocks were heated by exposure to the hot asthenosphere of the mantle wedge leading to development of open *P–T–t* loops, whereas markers within the continental crust show tighter *P–T–t* loops at lower temperatures within the HPM

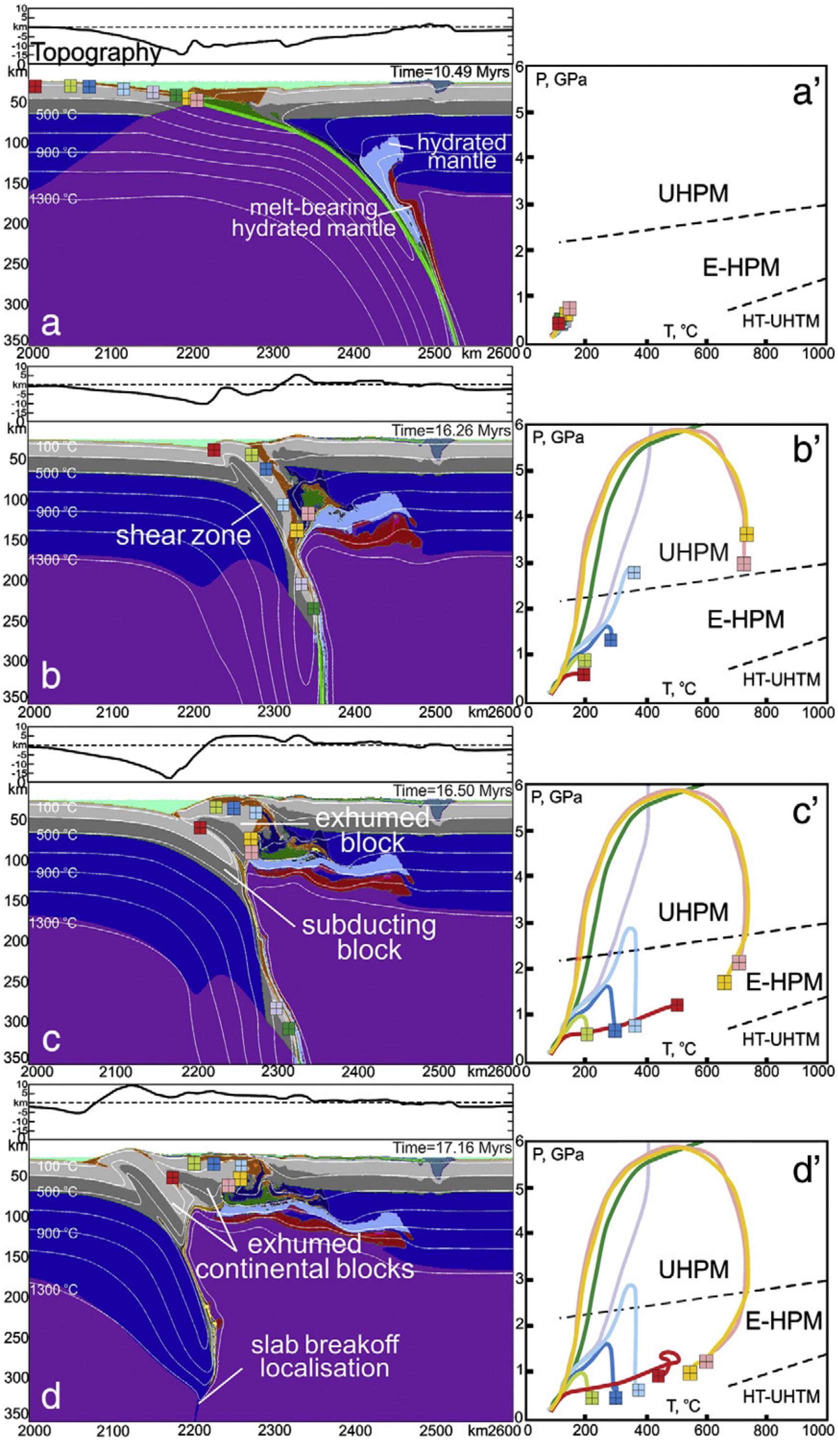

Fig. 2. Evolution of the reference model CS (large-scale crustal stacking; with the 600 km long oceanic lithosphere component and the abrupt (50 km wide) incoming passive margin). The model involves subduction of an oceanic plate (a) followed by subduction of the continental plate (b). The subducted continental crust decouples from the underlying lithospheric mantle as a block (b) and ascends close to the surface, whereas the continental lithosphere continues to subduct leading to decoupling of a second block of continental crust which ascends to underthrust the first (c). During the ascent of the second continental block, subduction is terminated by slab breakoff, which localizes in the continental part of the slab at a depth of 300 km (d). The topographic profile for each snapshot is given on the top. Colored squares on the snapshots are markers that refer to the diagrams with the *P–T–t* paths (a′–d′). The dashed lines separate fields of different types of metamorphism (Brown, 2007): UHPM = ultrahigh-pressure metamorphism; E–HPM = eclogite–high-pressure granulite metamorphism; and UHTM = ultrahigh-temperature metamorphism.

and UHPM *P–T* fields. The elevation of the orogen increases from the beginning of the exhumation stage and may reach up to 8 km.

Increasing the upper-mantle temperature to 60 K above the present value together with an increase in the lithosphere thickness (Lt = 150 km) and the mantle density contrast (D = 38 kg/m^3) leads to the appearance of a small area (about 50 × 50 km) of melt-bearing asthenosphere in the mantle wedge at the beginning of the collision stage due to overriding plate extension associated with mantle upwelling and decompression melting (Fig. 4a). The warmer environment allows deeper subduction of the continental material up to

~220 km depth compared to the previous model (~190 km). The subduction is terminated by slab breakoff, which localizes at the oceanic lithosphere–continental lithosphere transition at a depth of ~220 km (Fig. 4c). The breakoff results in a period of relaxation of the overriding continental plate, which causes a decrease in the temperature of the mantle wedge domain, which in turn leads to the cooling and crystallization of melt in the area of formerly melt-bearing mantle between the continental plates.

The sedimentary rocks (represented by green and blue markers) experience decompression partial melting during exhumation and form a complex structure at 10–30 km depth located between shallowly-subducted sedimentary rocks and the underlying continental crust on the left and hydrated mantle and the overlying volcanic rocks above and to the right (Fig. 4d). In contrast, although the subducted continental crust (represented by red, pink and purple markers) is exposed to HPM–UHPM conditions and returns coherently to the upper-middle crustal level by rapid eduction along its former subduction path in less than 1 million years, it does not melt. Delamination of the subducted subcontinental lithospheric mantle from the crust does not occur in this model. The exhumed HPM–UHPM units are located in the frontal area of the orogen at 10–30 km depth where the orogen has almost zero altitude, whereas the exhumed bending zone of the continental plate further to the left is characterized by an increased elevation of up to 7 km. The *P–T–t* paths for the subducted sedimentary rocks and continental crust are similar to those in the reference model.

A further increase in the upper-mantle temperature to 80–100 K above the present value, together with appropriate increases in the radiogenic heat production ($H_r = 1.5 \times H_r^0$), the lithosphere thickness (Lt = 160 km) and the mantle density contrast (D = 50 kg/m^3), leads to a completely different evolution of the model (Figs. 3d, e, 5, and S2 in Supplementary materials). Dehydration of the subducting slab and the effect of the prescribed high fluid pressure weaken the overriding plate, which undergoes extension associated with decompression partial melting of the mantle wedge. Early during the continental collision stage, conductive heating due to contact between the subducting slab and the hot asthenosphere of the mantle wedge causes weakening of the slab, which triggers shallow slab breakoff. Breakoff localizes at the oceanic lithosphere–continental lithosphere transition at a depth of ~100 km (Fig. 5b). In turn, there is a spontaneous rapid transition from subduction of the left-hand continental plate to retreat associated with extension of the initially thickened overriding continental margin. Since the left-hand continental plate is not fixed, the two continental plates start to diverge and the area of upwelling melt-bearing mantle grows laterally. Rapid syn- to post-collision extension of the overriding plate is associated with retreat of the left-hand continental plate and formation of an extensional basin with volcanic rocks.

As soon as the slab breakoff occurs, the continental crust (represented by yellow and pink markers) and the associated sedimentary rocks (represented by red and green markers), which had been subducted to a depth of ~80 km, are exhumed to the upper-middle crustal level (10–30 km depth) within the volcanic basin between the continental plates. Because of the fast evolution of the model, the exhumed rocks are not characterized by high temperatures, although the temperatures could increase further due to conductive heating from the underplating hot melt-bearing mantle, and the markers record open *P–T–t* loops, in most cases with a maximum temperature of ~500 °C (Fig. 5c′). The exhumed rocks are mostly characterized by eclogite–high-pressure granulite metamorphism (E–HPM), with the exception of one marker (pink) in the continental crust that just achieves high temperature metamorphism at UHPM conditions and returns to a depth of ~20 km. The collision zone is characterized by low altitude (see the topography profiles in Figs. 3d, e, and 5). Any further increase in the upper-mantle temperature does not change the style of the model evolution, but simply causes the formation of a larger melt-bearing area between the continents (Fig. 3f; Fig. S2 in Supplementary materials).

3.2. TD model: trans-lithospheric diapirism

3.2.1. Reference model for present-day conditions

An important parameter that has a significant influence on the evolution of the collision zone is the width of the incoming passive margin. In the CS model described above the oceanic lithosphere is attached to the continental lithosphere against an abrupt passive margin only 50 km wide overlain by sedimentary rocks (see Fig. 2). In contrast, in reference model TD a gradual passive margin 150 km wide overlain by sedimentary rocks is introduced (Fig. 6a). The gradual passive margin allows deeper subduction of the continental plate (up to 250 km depth; Figs. 6c and S3c in Supplementary materials, also see Sizova et al., 2012) in comparison with the CS model (up to 200 km depth, Fig. 2) with its abrupt passive margin.

At a depth of 140–180 km the sedimentary rocks from the deeply subducted passive margin start to ascend, partly undergo partial melting, and form a diapir above the slab (Fig. 6c, d). This diapir rises vertically penetrating through the lithosphere of the overriding plate weakened by serpentinization during the subduction stage as well as by upward percolation of melts extracted from the diapir. During the ascent of the diapir sedimentary rocks mix with hydrated lithospheric mantle of the overriding plate forming a strongly internally deformed UHPM melange that is emplaced into the bottom of the crust. Similar trans-lithospheric sedimentary diapirs were found in oceanic subduction models when strong melt-induced weakening was implemented (Gerya and Meilick, 2011). The sedimentary rocks (represented by red, pink, green and blue markers) follow almost isothermal compression and decompression segments in the *P–T–t* evolution with maximum temperature not exceeding 700 °C at UHPM conditions (Fig. 6d′).

3.2.2. Extrapolation of the TD model back in time

Increasing the upper-mantle temperature for the TD model, leads to notable changes in the internal evolution and geometry of the continental collision zone (Figs. 7 and 8). Increasing the upper-mantle temperature to 100 K above the present value, together with appropriate increases in the radiogenic heat production ($H_r = 1.5 \times H_r^0$), the lithosphere thickness (Lt = 160 km) and the mantle density contrast (D = 50 kg/m^3), produces a geodynamic regime manifested by rapid overriding plate extension associated with decompression melting in the mantle wedge at the beginning of the continental collision stage (Fig. 8a). During subduction of the continental plate this area of melt-bearing mantle grows laterally up to about 100 × 100 km (Fig. 8b).

Less than 1 Ma after the collision stage was initiated the subduction is terminated by slab breakoff at moderate depth, which localizes at the oceanic lithosphere–continental lithosphere transition at ~200 km (Fig. 8b). The breakoff exerts an instantaneous influence on the system resulting in a period of extension of the initially thickened overriding continental plate, which is associated with eduction of the subducted continental plate (Fig. 8c, d). This causes a slight increase of the elevation of the orogen in the bending zone of the continental plate, while the area above the melt-bearing mantle represents a basin with ~2–3 km of volcanic rocks. No delamination of subducted continental mantle lithosphere from the crust occurs in this model.

The sedimentary rocks on top of the subducting plate (represented by red, green and pink markers) reach the UHPM field where they are in contact with the hot asthenosphere of the mantle wedge for long enough to undergo partial melting during eduction and overriding plate extension. They show mostly open *P–T–t* loops (Fig. 8). In contrast, rocks from the interior of the subducted and educted continental crust (represented by blue marker) were not heated to the same extent and are rapidly returned to the surface. Therefore, although they reach the UHPM field, they do so at extremely low temperatures of ~200–400 °C and are characterized by tight *P–T–t* loops (Fig. 8). The exhumed UHPM units are located at 10–20 km depth within a magmatic extensional basin formed in response to

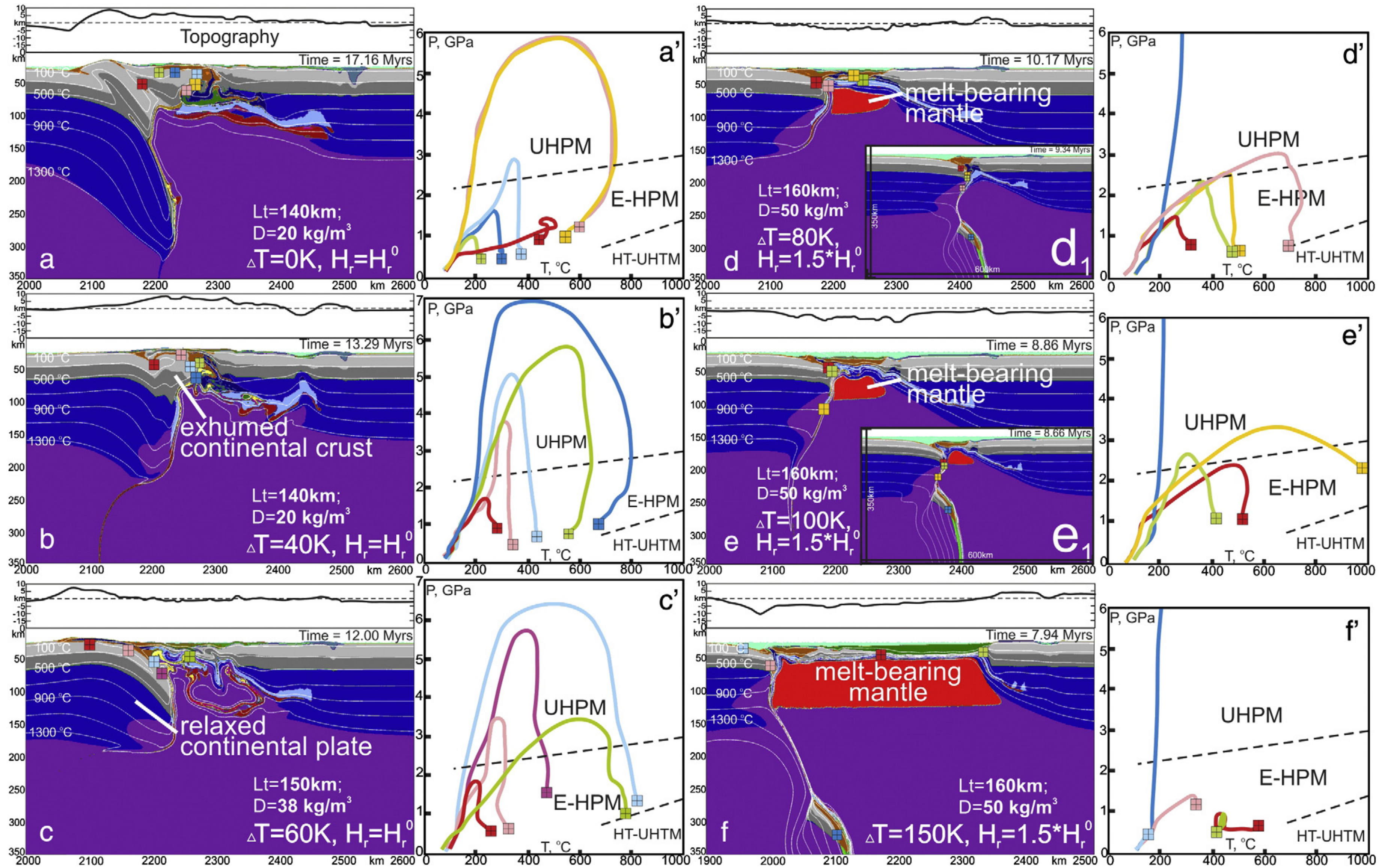

Fig. 3. Evolution of the CS model with increasing ambient upper-mantle temperature (ΔT), radiogenic heat production (H_r), thickness of the continental lithosphere (Lt), and density contrast between the subcontinental lithospheric mantle and the underlying mantle (D). Experiments show different regimes for continental collision (see Section 3.1.2), where UHPM rocks are formed in the *modern collision regime* at $\Delta T \leq 60$ K (a, b, c) but in the *truncated hot collision regime* at $\Delta T \geq 80$–100 K (d, e, f) the continental crust is not subducted to mantle depths and UHPM rocks are not produced.

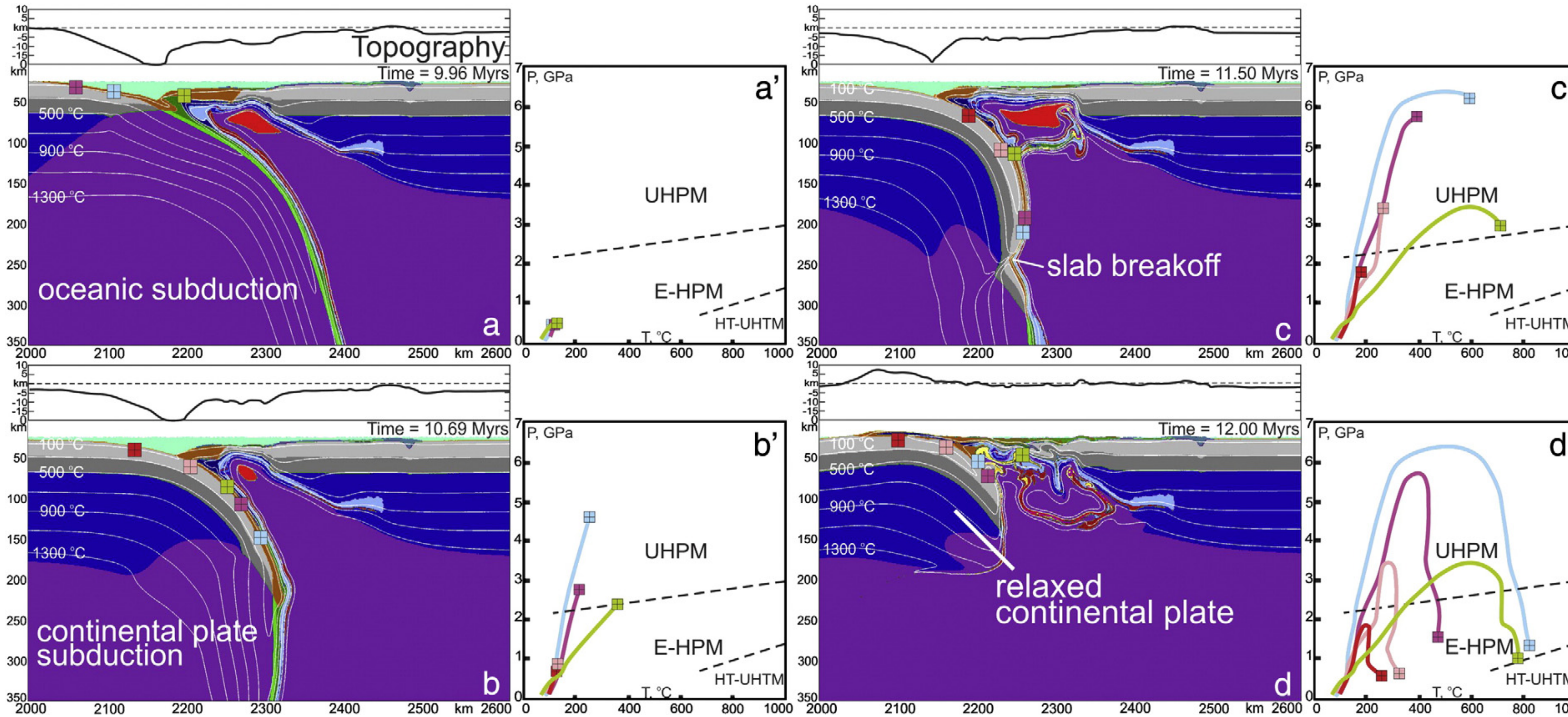

Fig. 4. Evolution of the CS model at $\Delta T = 60$ K; $H_r = H_r^o$; Lt = 150 km; D = 38 kg/m^3 (experiment from Fig. 3c). The model involves subduction of an oceanic plate (a) followed by subduction of the continental plate (b). A small area of melt-bearing asthenosphere from the mantle wedge forms between the two continental plates. Slab breakoff occurs at a depth of 220 km and causes the continental plate to relax with synchronous exhumation of sedimentary rocks undergoing decompression partial melting (c, d). The melt-bearing area formed at the beginning of the collision stage cools and crystallizes.

overriding plate extension associated with decompression melting of the asthenosphere of the mantle wedge rising beneath the basin.

A further increase in the upper-mantle temperature to 150 K above the present value, together with increasing the radiogenic heat production ($H_r = 1.5 \times H_r^0$), the lithosphere thickness (Lt = 160 km) and the mantle density contrast (D = 50 kg/m^3), leads to a formation of a larger area of melt-bearing mantle between the continental plates (Figs. 7c and S4 in Supplementary materials). Weakening of the subducting composite continent–ocean plate due to elevated upper mantle temperature results in a much shallower slab breakoff than in the previous experiment. This occurs at a depth of ~50 km in the continental part of the slab (~150 km from the oceanic lithosphere–continental lithosphere transition, Figs. 7c and S4c in Supplementary materials). A large fragment of the continental crust from the gradual passive margin detaches together with the slab, and both rapidly sink into the hot low-viscosity asthenosphere. Consequently, although crustal rocks comprising this fragment are exposed to UHPM conditions, they are not exhumed to the surface. In accordance with the high degree of magmatic and fluid weakening adopted, the overriding lithosphere over the area of the melt-bearing mantle is extended and a basin with ~5–15 km of volcanic rocks is developed. The thinned continental crust (represented by pink and red markers) records increasing temperature at constant pressure (Fig. 7c′).

3.3. VE model: vertical crustal extrusion

3.3.1. Reference model for present-day conditions

Fig. 9 (and Fig. S5 in Supplementary materials) illustrates the evolution of a model with an abrupt passive margin in which the length of the oceanic lithosphere component of the left hand plate is decreased to 400 km (compare with 600 km in the previous models; also see Sizova et al., 2012). Subduction of this lithosphere generates a weaker slab pull, slower convergence velocity, and more sluggish slab detachment during the spontaneous collision phase due to the decreased length of the oceanic plate (cf. Figs. S1c and S5b in Supplementary materials). The reference model VE results in the formation and exhumation of HT–UHPM crustal rock units with very high peak metamorphic temperatures (up to 1000 °C, Fig. 9c′).

At the beginning of the continental collision stage, after the ocean basin closes, as the incoming continental margin starts to subduct

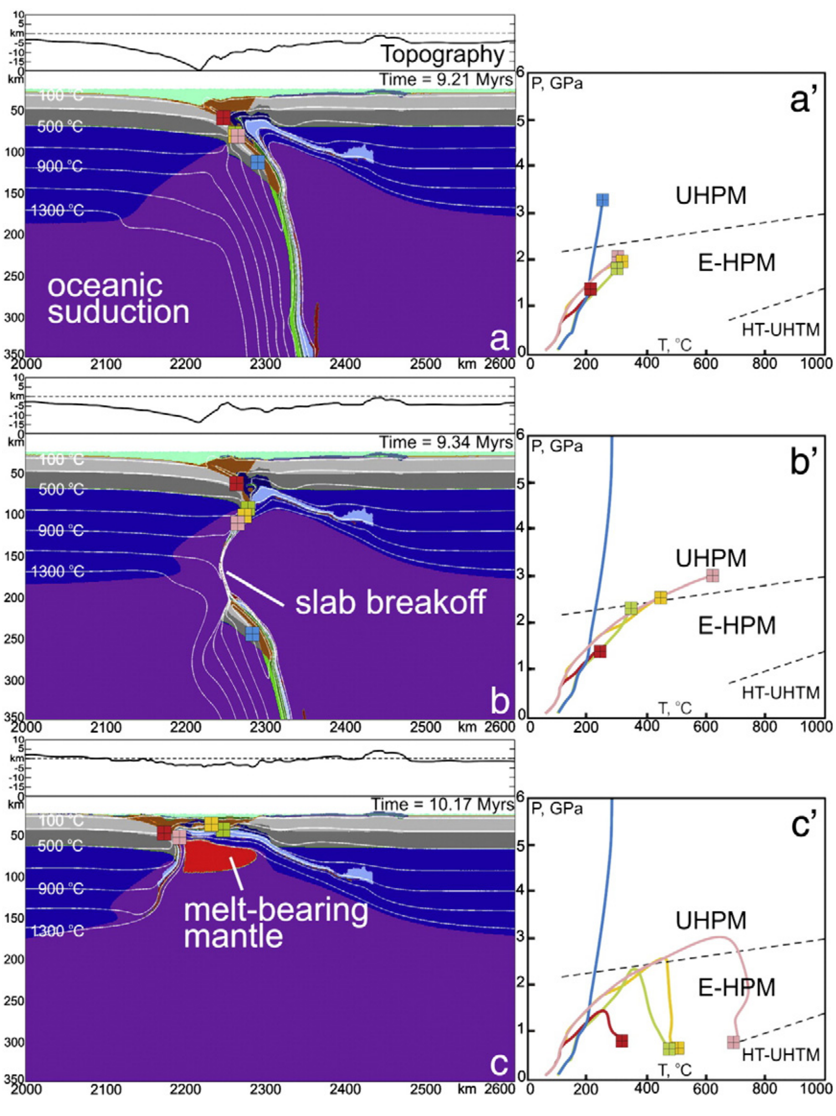

Fig. 5. Evolution of the CS model at $\Delta T = 80$ K; $H_r = 1.5 * H_r^0$; Lt = 160 km; D = 50 kg/m^3 (experiment from Fig. 3d). The model involves subduction of an oceanic plate (a) followed by subduction of the abrupt passive margin not deeper than 100 km (b). Slab breakoff occurs at a depth of 100–150 km. Melt-bearing asthenosphere from the mantle wedge forms between the two continental plates (c). The subducted sedimentary material is exhumed towards the surface (pink, yellow and green markers) but remains beneath the magmatic basin between the continental plates at a depth of 10–20 km.

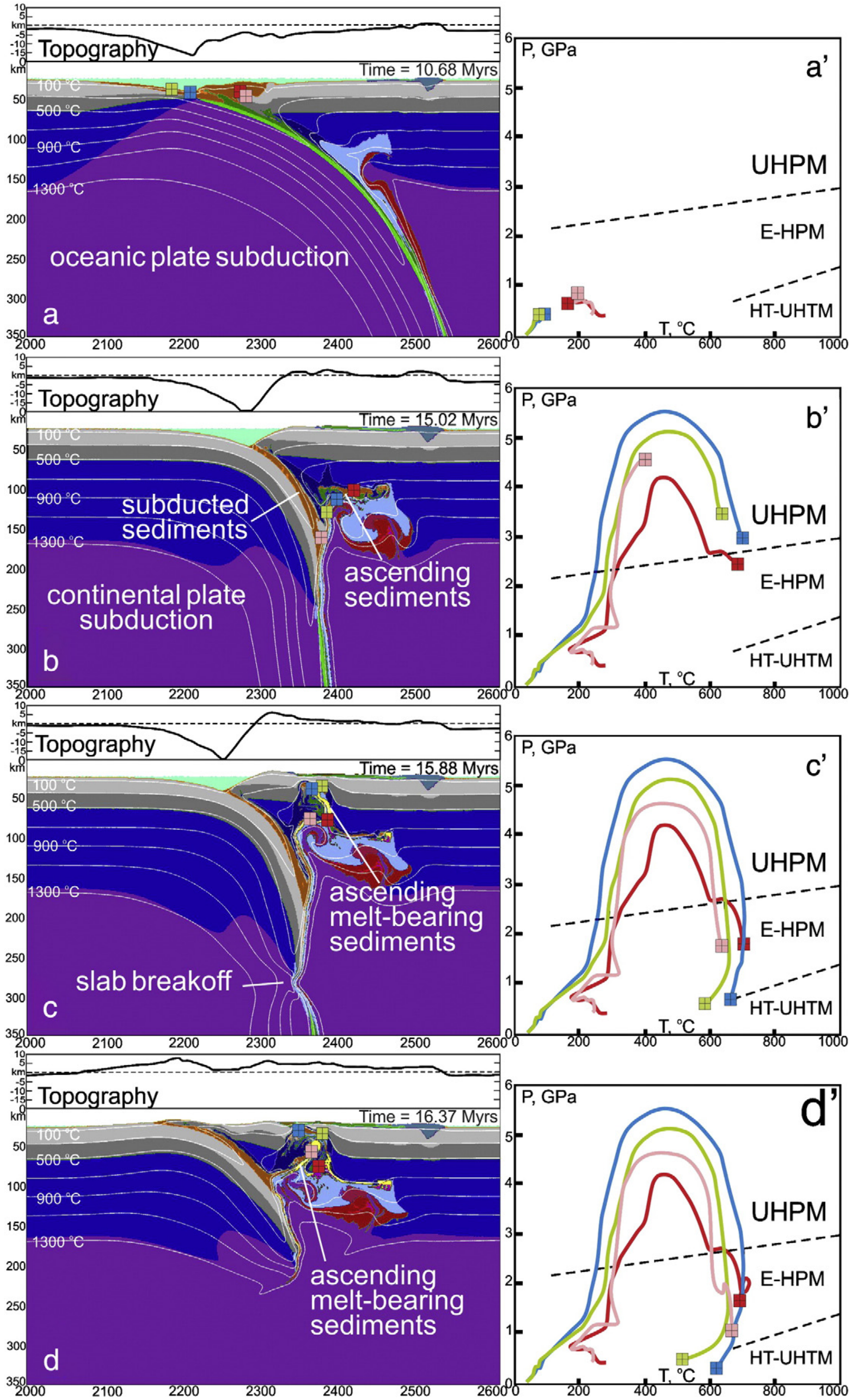

Fig. 6. Evolution of the reference model TD (trans-lithospheric diapirism; with the 600 km long oceanic lithosphere component and the gradual (150 km) passive margin). Subduction of the oceanic plate (a) is followed by subduction of the continental plate (b). As the subducted sedimentary rocks and the upper continental crust start to ascend, they undergo partial melting, and form a diapir above the slab (c, d). Slab breakoff occurs at the oceanic lithosphere–continental lithosphere transition at a depth of 250 km (c).

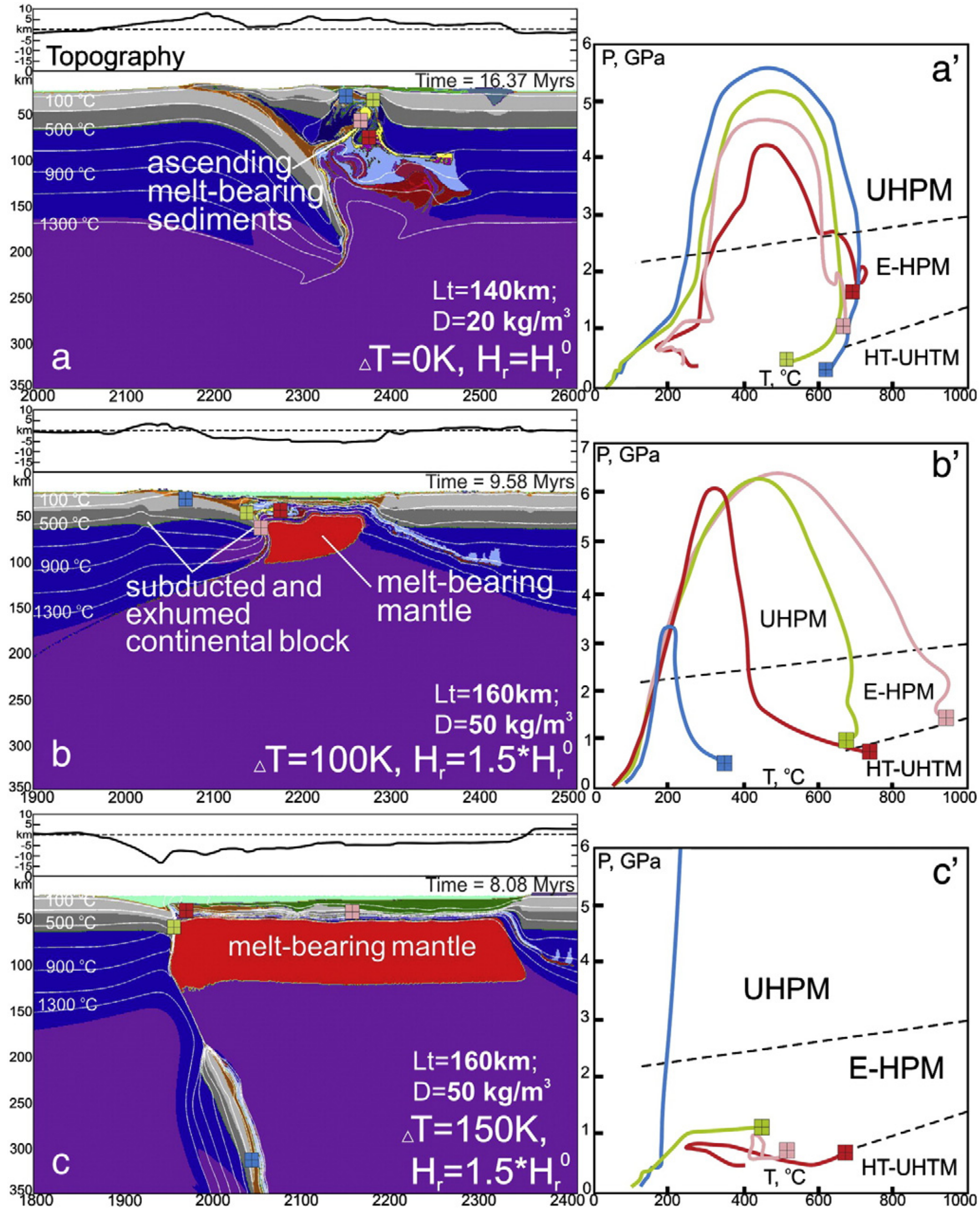

Fig. 7. Representative snapshots from the TD model with increasing ambient upper-mantle temperature (ΔT), radiogenic heat production (H_r), thickness of the continental lithosphere (Lt), and density contrast between the subcontinental lithospheric mantle and the underlying mantle (D). UHPM rocks are formed under present-day conditions (a) but the appearance of melt-bearing asthenosphere from the mantle wedge between the continental plates under the hotter conditions precludes formation of UHPM rocks (b, c) (for details see Section 3.2.2).

(Fig. 9a, b), the topographic elevation increases (see the topography profiles in Fig. 9) and the dip of the slab steepens to vertical (Figs. 9b, S5b in Supplementary materials). After the subducting continental lithosphere reaches a depth of ~60 km most of the upper continental crust starts to delaminate from the lower continental crust and accretes to the overriding plate within the subduction channel (Fig. 9b). The lower, rheologically stronger continental crust continues to be subducted, together with a thin remnant of the upper continental crust ~3 km thick.

The positive buoyancy of the subducting continental crust causes a gradual decrease in the subduction velocity that in turn triggers thermal relaxation of the subducting lithosphere. About 12 Ma after the collision stage was initiated subduction is terminated by slab breakoff, which does not localize at the oceanic lithosphere–continental lithosphere transition but occurs at a much greater depth of ~400 km in the oceanic part of the slab (Fig. S5b in Supplementary materials). The elevated slab temperature, which occurs in response to the slower subduction caused by the reduced slab pull of the short oceanic plate prescribed in the experiment, results in a viscous dripping instability in this model leading to slab detachment.

After the detachment, the weight of the remaining portion of the hanging slab is not sufficient to overcome the positive buoyancy of the continental crust, which ceases to subduct at ~200 km depth. The system remains essentially static for about 0.5 Ma and the deep detachment event does not exert any instantaneous influence on the system. A small component of slab rollback and extension of the overriding plate resume after the 0.5 Ma hiatus, leading to ascent of hot asthenosphere (Fig. 9c). In turn, this leads to smoothing of the high topography developed during the initial collision stage as the orogen widens (Fig. 9c, d).

During the period of slow continental subduction the continental crust is subjected to heating as the continental side of the vertically hanging slab comes into contact with the hot asthenosphere of the mantle wedge for a prolonged period of time (ca. 2 Ma), which allows conductive heating and partial melting of the remnant of upper

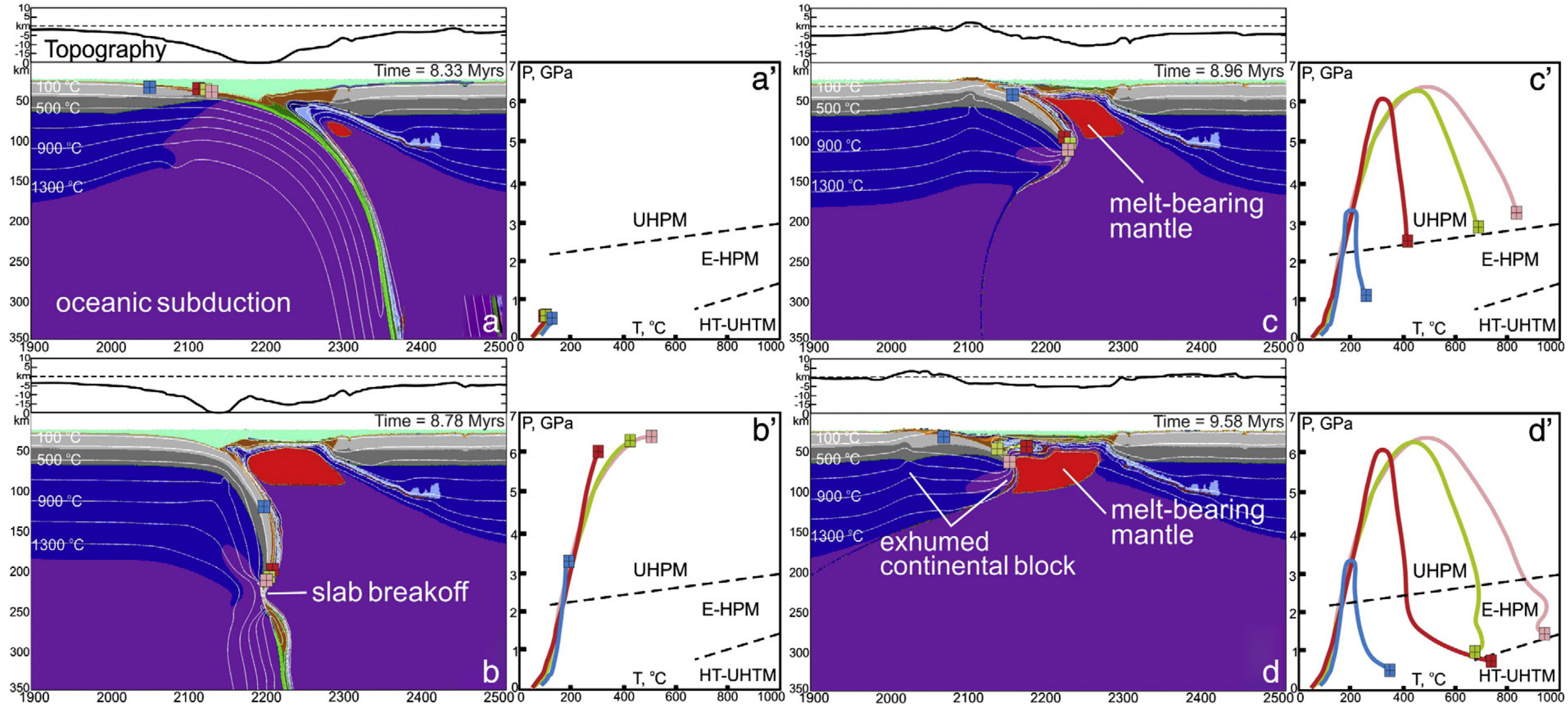

Fig. 8. Evolution of the TD model at $\Delta T = 100$ K; $H_r = 1.5 * H_r^o$; Lt = 160 km; D = 50 kg/m^3 (experiment from Fig. 7b). Subduction of the oceanic plate (a) is followed by subduction of the continental plate (b). An area of melt-bearing asthenosphere from the mantle wedge forms between the two continental plates. Slab breakoff occurs at a depth of ~200 km (b) and causes the continental plate to relax (c). The subducted continental plate returns to the surface along its subduction path (eduction). Subducted sedimentary material is exhumed to crustal depths but remains beneath the magmatic basin between the continental plates at a depth of 20–40 km.

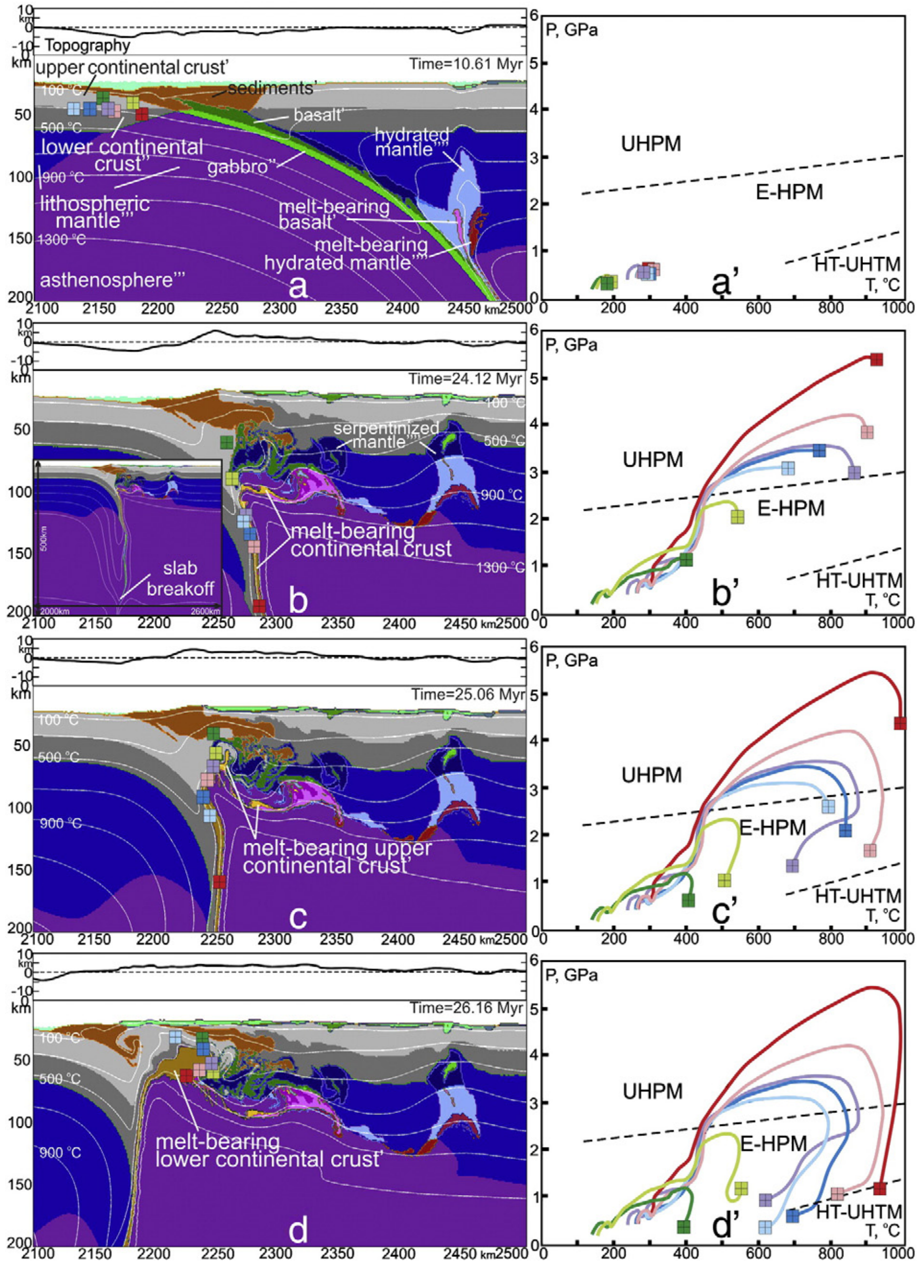

Fig. 9. Evolution of the reference model VE (vertical crustal extrusion; with the 400 km long oceanic lithosphere component and the abrupt (50 km wide) incoming passive margin). Subduction of the oceanic plate (a) is followed by subduction of the continental plate and partial melting of the continental crust and associated sedimentary materials (b, c, and d), which are then exhumed to middle-to-lower crustal depths (d).

continental crust and the lower continental crust at ultrahigh pressures. As a result, the positive buoyancy of the continental crust is enhanced and the overlying material becomes strongly weakened by the percolating UHP melts. This facilitates exhumation of the buoyant melt-bearing UHPM crustal rocks vertically towards the surface along the slab–mantle interface in the form of a gently curved planar or wave-like structure (Fig. 9c, d). The partially molten UHPM crust is exhumed to depths of 10–40 km forming a plume-like body ~50 km across in the bottom of the crust of the extending collision zone (Fig. 9d).

The *P*–*T*–*t* evolution of the subducted continental crust was tracked at several locations using markers (Fig. 9). During subduction all markers located in both the upper continental crust (represented by dark green, green and violet markers) and the lower continental crust (represented by blue, light blue, pink and red markers) show increasing pressure and temperature, whereas the decompression segments of the *P*–*T*–*t* paths are different. Some crustal material were subducted no deeper than ~140 km before being exhumed to middle crustal depths; these show tight *P*–*T*–*t* loops (e.g. violet and blue markers in Fig. 9). In contrast, more deeply subducted crustal materials, which finally underlie the early exhumed crustal materials at middle crustal depths (Fig. 9d′), have more open *P*–*T*–*t* loops with a larger segment of near-isothermal decompression close to peak temperature (e.g. red and pink markers). Parts of the upper continental crust that remained at temperatures below the solidus also become involved in the exhumation process and represent rocks that occur above and below the UHPM rocks in nature. These areas are characterized by high-pressure (dark green and green markers in Fig. 9) or lower-grade metamorphism.

3.3.2. Extrapolation of the VE model back in time

As in the previous models, increasing the upper-mantle temperature for the VE model, together with appropriate increases in the

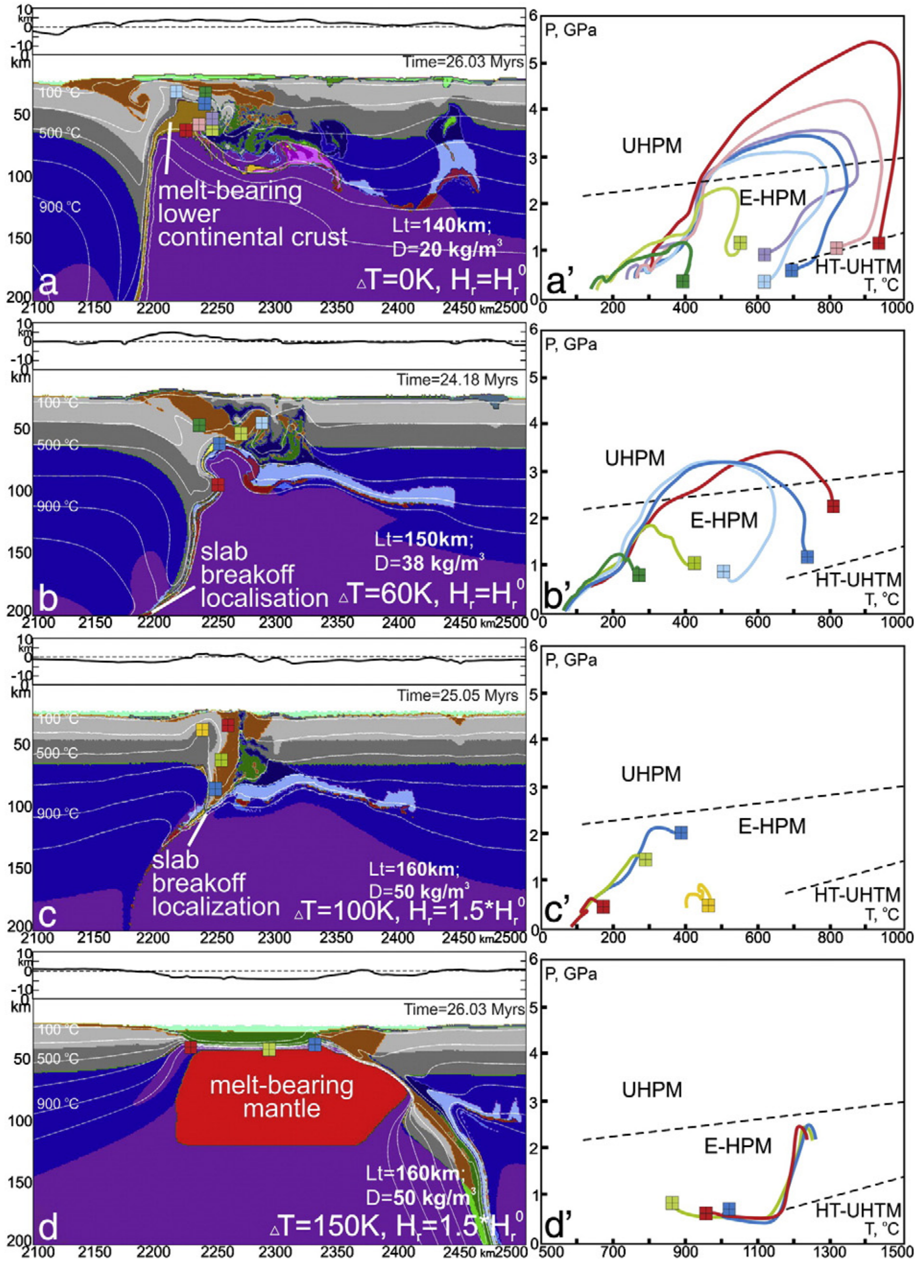

Fig. 10. Representative snapshots from the VE model with increasing ambient upper-mantle temperature (ΔT), radiogenic heat production (H_r), thickness of the continental lithosphere (Lt), and density contrast between the subcontinental lithospheric mantle and the underlying mantle (D). While experiments at $\Delta T \leq 60$ K (a, b) show formation of UHPM rocks, experiments at the higher ambient upper-mantle temperatures (c, d) develop the *truncated hot collision regime* with shallow slab breakoff and the formation of melt-bearing asthenosphere from the mantle wedge between the continental plates (for details see Section 3.3.2).

lithosphere thickness (Lt = 150–160 km) and the mantle density contrast (D = 38–50 kg/m^3), leads to shallower slab breakoff and precludes deep subduction of continental crust. UHPM rocks are no longer generated in models where the upper-mantle temperature is increased to more than 60 K above the present value, and slab breakoff occurs at the oceanic lithosphere–continental lithosphere transition at a depth of ~100 km (Figs. 10c and S6 in Supplementary materials) and terminates subduction. The breakoff results in a period of partial eduction of the subducted continental plate and relaxation and extension of the overriding plate. Where the subducted continental crust achieves UHPM *P–T* conditions (represented by the red marker) it develops an open *P–T–t* loop, but the UHPM crust remains at mantle depths and is not exhumed back to crustal depths (Fig. 10b). In contrast the associated sedimentary rocks that reached a depth of ~100 km (represented by the blue and light blue markers) experience UHPM *P–T* conditions and are exhumed back to middle-to-lower crustal depths along open *P–T–t* loops (Fig. 10b′), locally undergoing decompression partial melting.

At an upper-mantle temperature of 100 K higher than the present value, together with increases in the radiogenic heat production ($H_r = 1.5 \times H_r^0$), the lithosphere thickness (Lt = 160 km) and the mantle density contrast (D = 50 kg/m^3), the continental plates stick together forming a narrow collision zone. Less than 1 Ma after the collision stage was initiated the subduction is terminated by shallow slab breakoff, which localizes at the oceanic lithosphere–continental lithosphere transition at a depth of ~70 km and terminates continental subduction at this level (Fig. 10c). The subducted continental crust and associated sedimentary rocks (represented by the red, green and blue

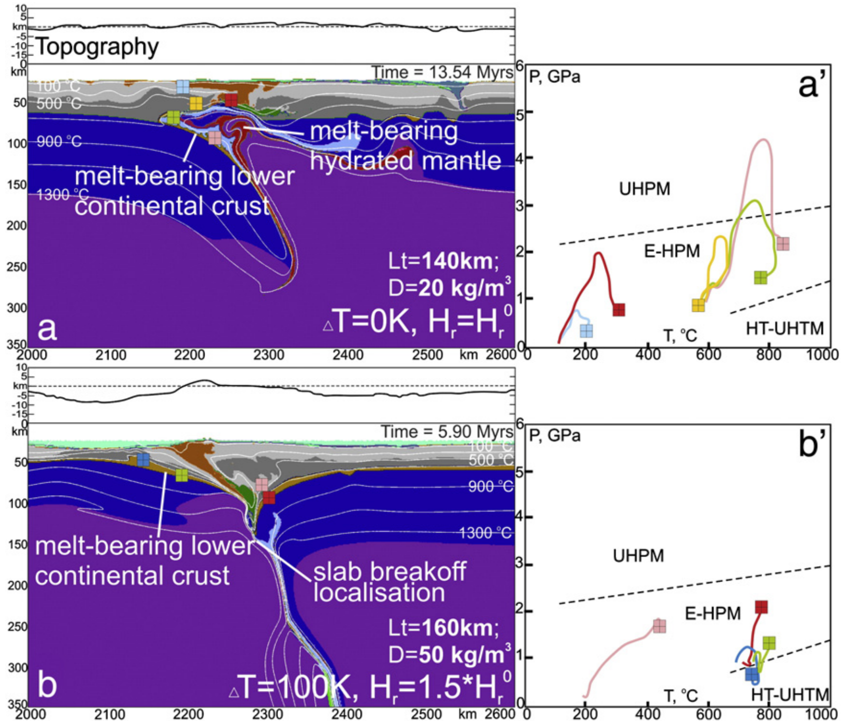

Fig. 11. Representative snapshots from the reference model SD (shallow crustal delamination; with the weak felsic lower continental crust with high radiogenic heat production and abrupt passive margin) under present-day conditions (a) and at the ambient upper-mantle temperature of 100 K higher than the present-day value (b). The weak lower continental crust prevents subduction of the continental crust under the present-day conditions, but the *two-sided hot collision regime* is developed at higher ambient upper-mantle temperatures (for details see Section 4.1.2).

markers) are caught within the narrow collision zone at a depth <60 km and record *P–T–t* paths within the eclogite–high-pressure granulite metamorphism (E–HPM) field (Fig. 10c′).

A further increase of the upper-mantle temperature to 150 K above the present value leads to the formation of a large area of melt-bearing mantle at the beginning of the collision stage (Fig. 10d). In contrast to the previous experiments at high upper-mantle temperatures, the area of melt-bearing mantle does not initiate between the two continental plates; instead it starts beneath the incoming passive margin as a consequence of the margin necking before the breakoff. As in the hot TD model experiments (Fig. 7c), a large fragment of the detached passive margin crust is subducted to UHPM depths to be lost in the mantle (Fig. 10d). Post slab breakoff extension produces a large basin with ~10 km of volcanic rocks between the two continental plates (Fig. 10d), similar to the results of the other hot collision experiments described above.

4. Experimental results for a model with weak felsic lower crust

4.1. SD model: shallow crustal delamination

4.1.1. Reference model for present-day conditions

In the previous reference models (with present-day upper-mantle temperature) a mafic composition with a relatively strong rheology (plagioclase, An75; Ranalli, 1995) was prescribed for the lower continental crust. This produced strong coupling during subduction between the continental crust and the subcontinental lithospheric mantle across the Moho boundary and enabled deep subduction of the continental crust into the UHPM field.

Reference model SD (shallow crustal delamination) is similar to reference model CS, but with a felsic lower continental crust with a weaker rheology (wet quartzite rheology; Ranalli, 1995) and higher radiogenic heat production (similar to the upper continental crust). The results of two experiments are reported. For both experiments the length of the oceanic lithosphere component of the left-hand plate is 600 km, but in the first experiment the width of the incoming passive margin was 50 km (abrupt passive margin) whereas for the second experiment the width of the incoming passive margin was 150 km (gradual passive margin). For this model with present-day upper-mantle temperature, very deep subduction of the continental crust does not occur in either experiment. Instead, in the first experiment (with the abrupt passive margin) at a depth of ~80 km the weak continental crust decouples from the underlying subcontinental lithospheric mantle (Fig. S7b in Supplementary materials), which continues to subduct causing buckling of the overlying continental crust. The same features occur in the second experiment (Fig. 12a).

Subduction of the subcontinental lithospheric mantle is terminated by slab breakoff, which localizes at the oceanic lithosphere–continental lithosphere transition at a depth of ~250 km in the first experiment (Fig. S7c in Supplementary materials). The breakoff results in a period of relaxation of the overriding continental plate. The hot asthenosphere from the mantle wedge penetrates along a weak zone between the subcontinental lithospheric mantle and the continental crust in both experiments (Figs. 11a and 12a), but less efficiently in the second experiment, extending the orogen and smoothing the topography. Very deep subduction of the continental crust and exhumation of UHPM rocks are precluded in these experiments. Markers tracking *P–T–t* paths in the first experiment into the UHPM field are exhumed only to lower crustal depths (Fig. 11a′). In these experiments with weak felsic lower crust, as well as in the CS model with strong mafic lower crust, delamination of continental crust from the subducting subcontinental lithospheric mantle appears to be a characteristic feature of modern-style collision.

4.1.2. Extrapolation of the SD model back in time

Increasing the upper-mantle temperature for the SD model to 100 K higher than the present value for both experiments produces a different style of collision compared to all of the other experiments

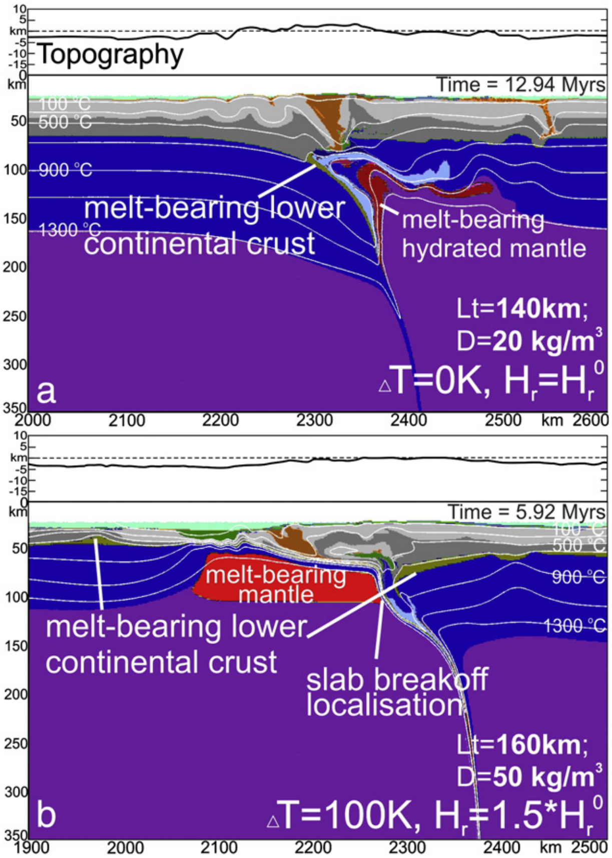

Fig. 12. Representative snapshots from the reference model SD (shallow crustal delamination; with the weak felsic lower continental crust with high radiogenic heat production and gradual passive margin) under present-day conditions (a) and at the ambient upper-mantle temperature of 100 K higher than the present-day value (b). The weak lower continental crust prevents subduction of the continental crust under the present-day conditions, but the *two-sided hot collision regime* is developed at higher ambient upper-mantle temperatures (for details see Section 4.1.2).

described above with higher upper-mantle temperatures. Coupling the higher radiogenic heat production for the felsic lower continental crust with the higher upper-mantle temperature in the SD model leads to a higher Moho temperature (>700 °C), which causes partial melting of the lower continental crust at the high initial geotherm (Figs. 11b and 12b; Fig. S8a in Supplementary materials).

During the early evolution of the first experiment (with the narrow passive margin, Fig. 11b) the melt-bearing lower continental crust forms a dome-like structure at the left side of the orogen as the ocean basin is closed by subduction of the oceanic lithosphere. This dome is noticeably stretched by the slab pull after the onset of collision (e.g. the blue marker in Fig. 11b′). At the beginning of the continental collision stage, the incoming continental lithosphere couples to the overriding plate and involves it in a short period of double-sided subduction. As a result, both continental plates subduct and create a broad and hot two-sided orogen with a strongly deformed and partially molten crustal root (Fig. 11b; Fig. S8b in Supplementary materials). The red and green markers in Fig. 11b′ show that the temperature reaches about 800 °C in the root of the orogen. Subduction of both continental plates is terminated by slab breakoff, which localizes at the oceanic lithosphere–continental lithosphere transition in the left hand plate at a depth of ~80 km under the central portion of the orogen. Slab breakoff is followed by a period of isostatic relaxation of topography and crustal extension within the orogen (Fig. S8c, d in Supplementary materials).

In the second experiment the introduction of a gradual passive margin leads to a slightly different evolution (Fig. 12b). A large area of melt-bearing mantle forms at the beginning of the collision stage beneath the incoming passive margin as a consequence of the margin necking before the breakoff (similar to the VE model with ambient upper-mantle temperature of 150 K higher than the present-day value). In a similar fashion to the first experiment, the incoming continental lithosphere couples to the overriding plate and involves it in a short period of double-sided subduction forming a hot two-sided orogen with a strongly deformed and partially molten crustal root (Fig. 12b). In contrast to the first experiment, this orogen is underlain by an area of melt-bearing mantle which maintains the hot environment at the collision zone. Slab breakoff localizes within the continental lithosphere at a depth of ~80 km and terminates continental subduction at this depth.

5. Discussion

5.1. Reference models

This study used a 2D petrological–thermomechanical numerical model for continental collision to investigate secular change in the style of collisional orogenesis. This model was previously used to investigate exhumation mechanisms of UHPM rocks during collision of spontaneously moving plates (Sizova et al., 2012). In the previous study the length of the subducting oceanic plate (=slab pull), the width of the passive margin (=geometry, abrupt or gradual) and the composition of the lower continental crust (=mafic or felsic, strong or weak) were varied in a series of experiments for present-day conditions of ambient upper mantle temperature, crustal radiogenic heat production, and thickness and chemical buoyancy of the continental lithosphere. The results of that study, which included fluid- and melt-induced weakening, confirmed that slab pull, geometry of the margin and strength of the lower continental crust were responsible for determining the dominant mechanism of exhumation of UHPM rocks (Sizova et al., 2012). The study identified a wide variation of exhumation mechanisms that correspond well with exhumation mechanisms proposed for UHPM rocks on the basis of both natural examples (e.g. Andersen et al., 1991; Kaneko et al., 2000; Wallis et al., 2005; Epard and Steck, 2008; Brueckner et al., 2010; Hacker et al., 2010) and analog modeling (e.g. Chemenda et al., 1995). Because the formation and exhumation of UHPM rocks is the characteristic feature of continental collision on modern Earth, the model conditions for the principal mechanisms of exhumation of UHPM rocks were selected as reference models for this study of secular change in the style of collisional orogenesis (Sizova et al., 2012).

The reference model CS with a long oceanic plate (600 km), an abrupt passive margin (50 km wide) and strong (mafic) lower crust shows fast stacking of rigid continental crustal blocks, which leads to duplication of the continental crust and the formation of UHPM materials at the frontal part of the suture zone (Fig. 2d, d′). This type of structure with duplication of the continental crust by intracontinental thrusting associated with coeval erosion is documented for several collisional orogenic systems, such as, for example, the western Alps (Schmid and Kissling, 2000), the Dabie Shan in China (Okay and Sengör, 1992; Okay et al., 1993; Yin and Nie, 1993; Nie et al., 1994) and the Western Gneiss Region in Norway (Hacker et al., 2010).

In the reference model TD with a gradual passive margin (150 km wide) rather than an abrupt passive margin, but still with a long oceanic plate and strong lower continental crust, exhumation of deeply subducted crustal and sedimentary materials, which undergo partial melting at UHPM conditions, occurs by trans-lithospheric diapirism (Fig. 6). Such a mechanism has been proposed for UHPM rocks in the Northern Tibetan Plateau, Northwest China in the Ordovician–Silurian (Yin et al., 2007), in the Norwegian Caledonides in the Lower Devonian (Root et al., 2005), in the Dabie Shan, eastern China in the Triassic (Wang and Cong, 1999), in the south-eastern Pamir in the

Eocene–Miocene (Hacker et al., 2005), and in the D'Entrecasteaux Islands, Papua New Guinea in the Miocene–Pliocene (Little et al., 2011), and is expected to occur in many arcs (Behn et al., 2011).

In contrast, in the model with the shorter oceanic plate (400 km) and an abrupt passive margin and strong lower continental crust (reference model VE) exhumation of buoyant melt-bearing UHPM rocks occurs by ascent along the slab–mantle interface by a process of vertical crustal extrusion (Fig. 9). The formation of a plume-like body ~50 km across in the bottom of the crust of the extending collision zone is similar to that suggested for the Sulu terrane by Wallis et al. (2005). In agreement with nature, HT–UHPM rocks in the model are located within high-pressure but lower-grade metamorphic units bounded by sharp tectonic contacts ('intrusive-like', e.g. Wang et al., 1997).

The results of these numerical experiments for present-day conditions cover a large proportion of the full range of *P*–*T* conditions documented from UHPM rocks, particularly for HT–UHPM rocks. The highest peak metamorphic temperatures (up to 1000 °C) are recorded in the case of vertical crustal extrusion (reference model VE) in which subducted continental crust in the vertically hanging slab is subjected to prolonged heating by contact with the hot asthenosphere of the mantle wedge. For this type of evolution with the formation and exhumation of UHPM rocks, the term *modern collision regime* is proposed.

5.2. Secular change in collisional orogenesis

For each of the reference models the ambient upper-mantle temperature, crustal radiogenic heat production, and thickness and chemical buoyancy of the continental lithosphere were increased in a stepwise fashion until conditions appropriate for the Proterozoic were achieved. For the CS model (Fig. 3), even a slight increase in upper-mantle temperature to 40 K above the present-day value precludes stacking of rigid continental crustal blocks and duplication of the continental crust. Nonetheless, the sedimentary and crustal materials are subducted to great depth (~190 km), exposed to UHPM conditions and returned to crustal depths. An experiment with an upper-mantle temperature of 60 K higher than the present-day value shows similar results, with deep continental subduction and formation of UHPM rocks. Since this evolution allows the formation and exhumation of UHPM rocks, even though the upper-mantle temperature has been increased above the present-day value, the term *modern collision regime* remains appropriate. Given that the ambient upper-mantle temperature was still ~60 K warmer at the beginning of the Phanerozoic Era (Labrosse and Jaupart, 2007; Herzberg et al., 2010), the *modern collision regime* applies to collisional orogenesis throughout the Paleozoic Era.

Although strong mafic lower crust plays an important role in collision models for present-day conditions, particularly for the formation and exhumation of UHPM rocks, it plays a lesser role in experiments with higher ambient upper-mantle temperatures appropriate for the Precambrian. For the CS model, an upper-mantle temperature of 80–100 K higher than the present-day value precludes deep subduction of the continental crust and formation of UHPM rocks (Fig. 3). Instead shallow slab breakoff occurs followed by post-collisional extension that produces a basin underplated by hot melt-bearing mantle. For an upper-mantle temperature of 150 K higher than the present-day value the post-collisional extension is more intense (Fig. 3). For this type of evolution without the formation of UHPM rocks, the term *truncated hot collision regime* is proposed (e.g. Figs. 3d, e, f, 7b, c, 8 and 10d). This is one style of collisional orogenesis that applies to Proterozoic Era.

Delamination of the subducted subcontinental lithospheric mantle from the crust, which is common in modern style collision models (Figs. 3a, 11a, and 12a), does not occur in the investigated hotter collision models (Figs. 3e, f, 11b, and 12b). Also, in the experiments resulting in development of the *truncated hot collision regime* the collision zones are characterized by negative topographic relief; this is consistent with results from the numerical experiments of Rey and Houseman (2006), who showed that convergence involving warm and buoyant lithosphere results in less topographic relief.

Early, shallow slab breakoff was previously suggested by van Hunen and Allen (2011) as the feature of hot collision regimes that would prohibit formation of UHPM rocks in the Precambrian. At higher ambient upper-mantle temperatures slabs are weaker than at present (van Hunen and van den Berg, 2008; Sizova et al., 2010). Furthermore, the presence of melt-bearing asthenosphere between the continental plates in the *truncated hot collision regime* could make the subducting plate-bending zone even weaker due to conductive heating and contribute to easier slab detachment at shallow depths. In experiments where shallow slab breakoff was localized inside the subducting continental plate, large fragments of the detached passive margin crust were subducted to UHPM depths, but since these remained attached to the sinking slab they were lost to the deep mantle leaving no geological record at the surface (Figs. 7c and 10d).

For the TD model with a gradual passive margin, an increase of the upper-mantle temperature to 100 K above the present-day value leads to the development of melt-bearing asthenosphere within the collision zone. However, in this case the gradual passive margin facilitates subduction of the continental crust to mantle depths. Slab breakoff occurs at a depth of ~200 km and results in eduction of the continental plate (Fig. 8). Although the continental crust does reach UHPM conditions it is only exhumed to the Moho where it remains buried under the volcanic basin that formed due to the presence of the melt-bearing asthenosphere. If the upper-mantle temperature is increased to 150 K above the present-day value, subduction of the continental crust to UHPM conditions is no longer possible and a larger volcanic basin forms due post-collisional extension and decompression melting of the mantle beneath the overriding plate.

For the VE model with an abrupt passive margin, a 400 km long oceanic plate and an ambient upper-mantle temperature of 100 K higher than the present-day value a different style of collision also develops. Slab breakoff is shallow, but melt-bearing asthenosphere does not develop between the continental plates at this stage (Fig. 10c). This may be due to the weak slab pull (proportional to the length of oceanic plate) prescribed in the experiment, which precludes initial extension of the overriding plate and decompression melting of the mantle, as occurs in other experiments that generate the *truncated hot collision regime* at the same ambient upper-mantle temperature. In the case of this particular VE model, further increase in the upper-mantle temperature to 150 K higher than the present-day value leads to the appearance of a zone of melt-bearing mantle beneath the incoming passive margin (Fig. 10d). In these experiments the high ambient upper-mantle temperature either precludes deep subduction of the continental crust and the development of UHPM rocks (Fig. 10c) or it prevents their return to crustal depths (Fig. 10d).

The most important parameters controlling the collision style at higher ambient upper-mantle temperatures are the rheology and radiogenic heat production of the lower continental crust. In experiments with a weak felsic lower crust (the SD model with ambient upper-mantle temperature of 100 K higher than the present-day value), the higher radiogenic heat production of the crust and the higher upper-mantle temperatures lead to formation of collision zones with a broad symmetrical orogenic wedge and a strongly deformed crustal root under which shallow slab breakoff is localized (Figs. 11b and 12b). In the experiment with a gradual passive margin, melt-bearing mantle appears beneath the incoming continental plate and maintains the hot environment at the orogenic wedge (Fig. 12b). UHPM rocks are not produced in this regime; instead partial melting of the lower continental crust leads to the formation of granites associated with amphibolite to granulite facies metamorphism (Fig. 11b, b′), features that are typical of many orogens from the Neoarchean to the Cambrian (e.g. Brown, 2007). For this type of evolution the term *two-sided hot collision regime* is proposed. This is another style of collisional orogenesis that applies to Proterozoic Era.

The calculated Moho temperature for the experiment using the SD model with ambient upper-mantle temperature of 100 K higher than the present-day value is >700 °C. At this temperature Burov and Yamato (2008) proposed that the 'crème brulée' model of lithosphere rheology is applicable with the development of Raleigh–Taylor instabilities in the subcontinental lithospheric mantle. Although the numerical models of Burov and Yamato (2008) do not include melting, the models demonstrate that at these conditions the continental crust could not be subducted to mantle depths. Instead, the continental crust of the overriding plate thickens at the collision zone.

The results of the experiments reported for the models tested in this study show that exhumation of UHPM rock units to shallow crustal depths in orogens could only have occurred at ambient upper-mantle temperatures <80–100 K higher than the present-day value. This is the threshold condition that allows slab breakoff to occur at a sufficient depth that the continental crust has reached UHPM conditions in the mantle before the detachment event. Thus, from the point in the thermal evolution of Earth when the ambient upper-mantle temperature declined to <80–100 K higher than the present-day value continental lithosphere with strong lower crust has been able to penetrate into the mantle to UHPM conditions and also be returned to shallow crustal depths to become part of the geological record. The timing of this change corresponds to sometime during the Neoproterozoic Era (Korenaga, 2006; Labrosse and Jaupart, 2007; Herzberg et al., 2010), which coincides with the second transition in the thermal structure of orogenic systems proposed by Brown (2006, 2007), during which blueschists and UHPM rocks appear for the first time in the geological record. Thus, the modeling presented here provides an explanation for why these rocks, which are the distinctive feature of Phanerozoic collisional orogens, are generally absent from Precambrian collisional orogens.

5.3. A comparison between Precambrian orogens and the numerical models

In contrast to Eoarchean–Mesoarchean crustal provinces, which register low-to-moderate-P–moderate-to-high-T metamorphism, collisional orogens from the Mesoarchean–Neoarchean to the Neoproterozoic–Cambrian are characterized by two contrasting types of metamorphism. Sutures are marked by eclogite–high pressure granulite metamorphism (E–HPM), where the maximum *P* of metamorphism increases to around 2 GPa by the mid-Paleoproterozoic (Brown, 2006, 2007) and apparent thermal gradients are generally in the range 350–700 °C/GPa. Away from sutures, these orogens are characterized by granulite facies and ultra-high temperature metamorphism (UHTM), with apparent thermal gradients that are generally in the range 800–1300 °C/GPa. The appearance of E–HPM and UHTM in the geological record since the Mesoarchean–Neoarchean registers a change in tectonics that generated sites of lower heat flow, inferred to be associated with subduction and the eventual orogenic suture, and sites of higher heat flow, corresponding to the orogenic hinterland. This fundamental change in tectono-metamorphic regime reflects the establishment of a steady-state mobile lid or plate tectonics regime on Earth (Sizova et al., 2010).

The common occurrence of ultra-high temperature metamorphism (UHTM) in Precambrian orogens corresponds to the general predictions from the *truncated hot collision regime* in the numerical models (Figs. 3d, e, f, 5, 7b, c, 8 and 10d). In the *truncated hot collision regime*, after collision and slab breakoff melt-bearing mantle develops systematically between the continental plates as they diverge from each other, and magma underplates the developing extensional basin. In these models, after the left-hand continent reaches the trench the push from the left edge is discontinued and subduction is driven spontaneously by slab pull; thus, after slab breakoff the left hand plate is no longer pulled into the mantle and extension is not limited by any push from the left hand edge of this plate. Syn-extensional magmatism results in the infilling of the extensional basin with volcanic rocks and maintains high-temperature conditions in the crust beneath the basin (Figs. 3f, 7c and 10d).

This type of deep hot crustal environment is typical for some long-lived Precambrian plutono-metamorphic orogens, such as the Neoarchaean Minto block in the northern Superior province of Canada (e.g. Bedard, 2003) and the late Mesoproterozoic Musgrave province central Australia (e.g. Smithies et al., 2011). Some Proterozoic orogens record post-extension thickening to generate counter-clockwise metamorphic *P–T* paths followed by slow close-to-isobaric retrograde cooling, such as occurred in the Paleoproterozoic Khondalite belt in the North China craton (e.g. Santosh et al., 2009; Tsunogae et al., 2011; Santosh et al., 2012) and the late Mesoproterozoic–early Neoproterozoic Eastern Ghats province (EGP), part of the Eastern Ghats belt (EGB) of peninsular India (e.g. Dasgupta et al., 2012; Gupta, 2012; Korhonen et al., in press). Such orogens might form by closure of the extensional basin formed in the *truncated hot collision regime*.

Taking the last example in more detail, the EGB exposes a deep crustal section through a composite Proterozoic orogen (Dasgupta et al., 2012; Gupta, 2012). Geological and isotopic data have been used to distinguish four discrete crustal provinces with contrasting histories within the EGB (Rickers et al., 2001; Dobmeier and Raith, 2003). The EGP is located in the central and northern parts of the EGB. The EGP records a single long-lived high-grade metamorphic evolution in the interval ca. 1130 Ma to ca. 900 Ma. The dominant rock types within the province include migmatitic sillimanite–garnet-bearing gneisses (referred to locally as khondalites), orthopyroxene-free garnetiferous quartzofeldspathic gneisses (referred to locally as leptynites), orthopyroxene-bearing charnockitic and enderbitic quartzofeldspathic gneisses, and two-pyroxene mafic granulites. Small lenses of calc-silicate and high Mg–Al granulites occur in the gneisses and record ultrahigh temperature metamorphic conditions. Although evidence for the UHTM is only preserved locally, the spatial distribution of the localities indicates that the event affected the entire EGP.

The timing of peak UHTM is estimated to be older than 980 Ma and possibly as old as 1042 ± 41 Ma (Korhonen et al., 2011, in press), consistent with the estimate of 1030–990 Ma from Bose et al. (2011), with a counter-clockwise evolution reaching peak *P–T* conditions of >950 °C and ~8 kbar (Korhonen et al., 2011, in press). These peak metamorphic conditions preceded the emplacement of regionally extensive charnockite–enderbite magmas at ca. 980 Ma. The predominant zircon and monazite age populations across the region in the interval ca. 980–930 Ma record the immediate post-peak evolution, characterized by slow close-to-isobaric cooling at a rate of ~1 °C/My from peak G-UHTM conditions to the elevated solidus at ~7.5 kbar. Ages younger than ca. 930 Ma are more enigmatic, but may be related to the release of fluids associated with final melt crystallization at depth during the waning stages of this tectono-metamorphic event.

A combination of a counter-clockwise *P–T* evolution with extremely high temperatures at moderate pressures suggests additional heat flux from the mantle, possibly by replacement of the lithospheric mantle with melt-bearing asthenospheric mantle during early extension prior to contractional thickening during the evolution to peak *T* and subsequent close-to-isobaric cooling. A scenario that requires early extension with extremely high temperatures is similar to the development of the *truncated hot collision regime* after slab breakoff in models CS and TD with an upper mantle temperature of 150 K above the present value and radiogenic heat production of 1.5 times the present value (Figs. 3f and 7c). These values are appropriate for the late Mesoproterozoic (Herzberg et al., 2010). In these models, during the subduction phase dehydration of the slab weakens the overriding plate, which undergoes extension associated with decompression partial melting of the mantle wedge and replacement of the subcontinental lithospheric mantle by hot, melt-bearing asthenospheric mantle. A renewed push from the left edge of the left-hand plate in these models would generate UHTM conditions during a counter-clockwise *P–T–t* evolution that would return the crust to 'normal' thickness consistent with a slow, close-to-isobaric retrograde *P–T–t* evolution.

Other Proterozoic orogens are characterized by clockwise looping metamorphic *P–T–t* paths and extensive granite magmatism derived from metasedimentary and metaigneous sources. These orogens have similarities with the *two-sided hot collision regime* in the numerical models (Figs. 11b and 12b), particularly the extensive lower crustal melting. Examples include the Paleoproterozoic orogen of the southwestern United States, comprising the Mojave, Yavapai and Mazatzal provinces (e.g. Karlstrom and Williams, 2006; Dumond et al., 2007), and the Paleoproterozoic Svecofennides of southern Finland (e.g. Korja et al., 2006; Cagnard et al., 2007; Kukkonen and Lauri, 2009).

Taking the last example in more detail, the Paleoproterozoic evolution of the Svecofennian orogen in the Fennoscandian shield comprised five tectonic events: continental rifting, microcontinent accretion, extension of the accreted crust, continent–continent collision, and extensional collapse of the collision belt (Lahtinen et al., 2005). Across southern Finland, the continent–continent collision at 1.85–1.79 Ga is characterized by migmatites and granites that were made famous by Sederholm during the early twentieth century (Sederholm, 1967; see also, Ehlers et al., 1993; Kurhila et al., 2005). The associated metamorphism is of high *T*/low *P* type (e.g. Korsman et al., 1984; Väisänen et al., 2002; Mouri et al., 2005) with looping *P–T–t* paths reaching amphibolite to granulite facies conditions (4–6 kbar, 650–800 °C) throughout southern Finland (e.g. Cagnard et al., 2007). The geochemistry of the granites requires a diverse range of metasedimentary and plutonic crustal sources, as well as in some cases hybridization between strongly enriched mantle-derived melts and anatectic melts derived from the Svecofennian crust (e.g. Kurhila et al., 2010, 2011; Rutanen et al., 2011). Late stage small, post-collisional (1.81–1.77 Ga) shoshonitic granites are strongly enriched in large ion lithophile elements and light rare earth elements, but relatively depleted in high field strength elements and heavy rare earth elements. The most likely origin for these magmas was by melting of the subcontinental lithospheric mantle, which had been enriched during the previous Svecofennian subduction–accretion process (Väisänen et al., 2000; Rutanen et al., 2011), as hot asthenosphere replaced the lower part of the lithosphere during limited orogenic collapse that left the crust thicker than average at the end of the orogenic event.

A combination of high *T*/low *P* type metamorphism with looping *P–T–t* paths reaching the granulite facies, but not ultrahigh temperature metamorphic conditions, with the widespread development of migmatites and granites suggests that crustal thickening provided the main source of heat for the extensive crustal melting. Advective and latent heat brought by the melts further increased the temperatures at the emplacement depth and contributed to the development of low-*P* granulite facies metamorphism (Kukkonen and Lauri, 2009). This scenario is reminiscent of the SD models in which the upper mantle temperature was raised to 100 K higher than the present (Figs. 11b and 12b). Coupling higher radiogenic heat production throughout the crust with the higher upper-mantle temperature leads to a higher Moho temperature (>700 °C), which causes partial melting of the lower continental crust at the high initial geotherm. Because the incoming continental lithosphere couples to the overriding plate and involves it in a short period of double-sided subduction both continental plates subduct to create a broad hot orogen with a partially molten crustal root where the temperature reaches about 800 °C. Subduction of both continental plates is terminated by slab breakoff, which is followed by a period of isostatic relaxation of topography and crustal extension within the orogen. In case of the experiment with the SD model, which used a gradual passive margin, the orogen is underlain by an area of melt-bearing mantle at shallow depth (Fig. 12b). Impingement of the hot asthenosphere against the thinned subcontinental lithospheric mantle generates the late stage shoshonitic magmas.

It is only during the Neoproterozoic that sutures become marked by early high-pressure and/or ultrahigh pressure metamorphism with apparent thermal gradients <350 °C/GPa and maximum P >2.7 GPa, with younger E–HPM recording the terminal collision (Brown, 2006, 2007). Except for the orogenic belts associated with the amalgamation of Gondwana in the late Neoproterozic to Cambrian (Cawood and Buchan, 2007), UHTM is rare at the surface in Phanerozoic orogens, but may be inferred at depth in the hinterland of some active orogens. As we have shown in the previous section, this second fundamental change in tectono-metamorphic regime reflects a threshold in upper mantle temperature below which continental crust can be subducted to mantle conditions and returned to the orogenic crust. This behavior corresponds to the *modern collision regime* in the models.

6. Conclusions

In a series of experiments using a general 2D petrological–thermomechanical numerical model, models of oceanic subduction and continental collision for present-day conditions that result in different exhumation mechanisms for UHPM rocks were extrapolated back in time to examine how increases in ambient upper mantle temperature, crustal radiogenic heat production, and thickness and chemical buoyancy of the continental lithosphere affect the collision process. Whereas changes in the model parameters such as the length of the subducting oceanic plate (which determines the slab pull), the width of the passive margin (abrupt or gradual geometry, which determines the ease of subduction of the continental margin) and the composition of the lower continental crust (mafic or felsic, relatively strong or weak) lead to a variety of exhumation mechanisms for UHPM rocks for present-day conditions, these features play a minimum role in experiments with higher upper mantle temperature conditions relating to the Precambrian. An increase of the ambient upper-mantle temperature to >80–100 K above the present-day value leads to two distinct modes of collision that are different from the *modern collision regime* and for which the terms *truncated hot collision regime* (strong mafic lower continental crust) and *two-sided hot collision regime* (weak felsic lower continental crust) are proposed. Both hot collision regimes are associated with shallow slab breakoff that precludes formation of UHPM rocks. Based on models for the thermal evolution of Earth the ambient upper mantle temperature most likely declined below 80–100 K warmer than the present-day value during the Neoproterozoic. A change in the style of orogenesis from the *hot collision regimes* to the *modern collision regime* in the Neoproterozoic is consistent with the appearance of UHPM rocks at that time and provides an explanation for their absence from the geological record until the Neoproterozoic.

Supplementary data to this article can be found online at http://dx.doi.org/10.1016/j.gr.2012.12.011.

Acknowledgments

This work was supported by ETH Research Grants TH-12/05-3 and TH-0807-3 and SNF Research Grants 200021-113672/1 and 200021-116381/1.

References

Abbott, D., Burgess, L., Longhi, J., Smith, W.H.F., 1994. An empirical thermal history of the Earth's upper mantle. Journal of Geophysical Research 99, 13835–13850.
Ahäll, K.I., Connelly, J.N., 2008. Long-term convergence along SW Fennoscandia: 330 m.y. of Proterozoic crustal growth. Precambrian Research 161, 452–474.
Andersen, T.B., Jamtveit, B., 1990. Uplift of deep crust during orogenic extensional collapse — a model based on field studies in the Song-Sunnfjord region of western Norway. Tectonics 9, 1097–1111.
Andersen, T.B., Jamtveit, B., Dewey, J.F., Swensson, E., 1991. Subduction and eduction of continental crust: major mechanisms during continent–continent collision and orogenic extensional collapse, a model based on the south Norwegian Caledonides. Terra Research 3, 303–310.

Auzanneau, E., Vielzeuf, D., Schmidt, M.W., 2006. Experimental evidence of decompression melting during exhumation of subducted continental crust. Contributions to Mineralogy and Petrology 152, 125–148.
Avigad, D., Chopin, C., Le Bayon, R., 2003. Thrusting and extension in the southern Dora-Maria ultra-high-pressure massif (Western Alps); vie from below the coesite-bearing unit. Journal of Geology 111, 57–70.
Baumann, C., Gerya, T., Connolly, J.A.D., 2010. Numerical modelling of spontaneous slab breakoff dynamics during continental collision. In: Spalla, M.I., Marotta, A.M., Gosso, G. (Eds.), Advances in Interpretation of Geological Processes: Geological Society, London, Special Publications, 332, pp. 99–114.
Bedard, J.H., 2003. Evidence of regional-scale, pluton-driven, high-grade metamorphism in the Archean Minto Block, Northern Superior Province, Canada. Journal of Geology 111, 183–205.
Behn, M.D., Kelemen, P.B., Hirth, G., Hacker, B.R., Massonne, H.-J., 2011. Diapirs as the source of the sediment signature in arc lavas. Nature Geoscience 4, 641–646.
Bittner, D., Schmeling, H., 1995. Numerical modeling of melting processes and induced diapirism in the lower crust. Geophysical Journal International 123, 59–70.
Bose, S., Dunkley, D.J., Dasgupta, S., Das, K., Arima, M., 2011. India–Antarctica–Australia–Laurentia connection in the Paleoproterozoic–Mesoproterozoic revisited: evidence from new zircon U–Pb and monazite chemical age data from the Eastern Ghats Belt, India. Geological Society of America Bulletin 123, 2031–2049.
Brown, M., 1993. P–T–t evolution of orogenic belts and the causes of regional metamorphism. Journal of the Geological Society of London 150, 227–241.
Brown, M., 2001. From microscope to mountain belt: 150 years of petrology and its contribution to understanding geodynamics, particularly the tectonics of orogens. Journal of Geodynamics 32, 115–164.
Brown, M., 2006. Duality of thermal regimes is the distinctive characteristic of plate tectonics since the Neoarchean. Geology 34, 961–964.
Brown, M., 2007. Metamorphic conditions in orogenic belts: a record of secular change. International Geology Review 49 (3), 193–234.
Brown, M., 2008. Characteristic thermal regimes of plate tectonics and their metamorphic imprint throughout Earth history. In: Condie, K.C., Pease, V. (Eds.), When did Earth First Adopt a Plate Tectonics Mode of Behavior? The geological Society of America, Special paper, 440, pp. 97–128.
Brueckner, H.K., Carswell, D.A., Griffin, W.L., Medaris Jr., L.G., Van Roermund, H.L.M., Cuthbert, S.J., 2010. The mantle and crustal evolution of two garnet peridotite suites from the Western Gneiss Region, Norwegian Caledonides: an isotopic investigation. Lithos 117, 1–19.
Brun, J.-P., 2002. Deformation of the continental lithosphere: insight from brittle–ductile models. In: De Meer, S., Drury, M.R., De Bresser, J.H.P., Pennock, G.M. (Eds.), Deformation Mechanisms, Rheology and Tectonics: Current Status and Future Perspectives: Geological Society Special Publication, 200, pp. 355–370.
Burg, J.-P., Gerya, T.V., 2005. The role of viscous heating in Barrovian metamorphism of collisional orogens: thermomechanical models and application to the Lepontine Dome in the Central Alps. Journal of Metamorphic Geology 23, 75–95.
Burov, E., Yamato, P., 2008. Continental plate collision, P–T–t–z conditions and unstable vs. stable dynamics: insights from thermo-mechanical modeling. Lithos 103, 178–204.
Cagnard, F., Durrieu, N., Gapais, D., Brun, J.-P., Ehlers, C., 2006. Crustal thickening and lateral flow during compression of hot lithospheres, with particular reference to Precambrian times. Terra Nova 18, 72–78.
Cagnard, F., Gapais, D., Barbey, P., 2007. Collision tectonics involving juvenile crust: the example of the southern Finnish Svecofennides. Precambrian Research 154, 125–141.
Cagnard, F., Barbey, P., Gapais, D., 2011. Transition between "Archaean-type" and "modern-type" tectonics: insights from the Finnish Lapland Granulite Belt. Precambrian Research 187, 127–142.
Calvert, A.J., Sawyer, E.W., Davis, W.J., Ludden, J.N., 1995. Archean subduction inferred from seismic images of a mantle suture in the Superior province. Nature 670–674.
Campbell, I.H., Griffiths, R.W., 1992. The changing nature of mantle hotspots through time: implications for the chemical evolution of the mantle. Journal of Geology 92, 497–523.
Cawood, P.A., Buchan, C., 2007. Linking accretionary orogenesis with supercontinent assembly. Earth-Science Reviews 82, 217–256.
Cawood, P., Kröner, A., Pisarevsky, S., 2006. Precambrian plate tectonics: criteria and evidence. Geological Society of America Today 16, 4–11.
Chacko, T., 2003. Are there systematic differences between the metamorphic temperatures of Phanerozoic, Proterozoic, and Archean collisional orogens? [abs.]. Geological Association of Canada, Society of Economic Geologists Joint Meeting, Vancouver, B.C., Canada, Abstracts, 28, p. 66.
Chardon, D., Gapais, D., Cagnard, F., 2009. Flow of ultra-hot orogens: a view from the Precambrian, clues for the Phanerozoic. Tectonophysics 477, 105–118.
Chemenda, A.I., Mattauer, M., Malavieille, J., Bokun, A.N., 1995. A mechanism for syn-collisional rock exhumation and associated normal faulting: results from physical modelling. Earth and Planetary Science Letters 132, 225–232.
Choukroune, P., Bouhallier, H., Arndt, N.T., 1995. Soft lithosphere during periods of Archean crustal growth or crustal reworking. In: Coward, M.P., Ries, A.C. (Eds.), Early Precambrian Processes: Geological Society Special Publication, 95, pp. 67–86.
Clauser, C., Huenges, E., 1995. Thermal conductivity of rocks and minerals. In: Ahrens, T.J. (Ed.), Rock Physics and Phase Relations: AGU Reference Shelf, 3, pp. 105–126.
Condie, K.C., 2008. Did the character of subduction change at the end of the Archean? Constraints from convergent-margin granitoids. Geology 36, 611–614.
Condie, K.C., Kröner, A., 2008. When did plate tectonics begin? Evidence from the geologic record. In: Condie, K.C., Pease, V. (Eds.), When did Earth First Adopt a Plate Tectonics Mode of Behavior? The geological Society of America, Special paper, 440, pp. 281–294.
Condie, K.C., Kröner, A., 2013. The building blocks of continental crust: evidence for a major change in the tectonic setting of continental growth at the end of the Archean. Gondwana Research 23, 394–402.
Condie, K.C., O'Neill, C., 2010. The Archean–Proterozoic boundary: 500 my of tectonic transition in Earth history. American Journal of Science 310, 775–790.
Condie, K.C., Pease, V. (Eds.), 2008. When did Earth First Adopt a Plate Tectonics Mode of Behavior? The Geological Society of America, Special Paper, 440, p. 294.
Connolly, J.A.D., 2005. Computation of phase equilibria by linear programming: a tool for geodynamic modelling and its application to subduction zone decarbonation. Earth and Planetary Science Letters 236, 524–541.
Dasgupta, S., Bose, S., Das, K., 2012. Tectonic evolution of the Eastern Ghats Belt, India. Precambrian Research. http://dx.doi.org/10.1016/j.precamres.2012.04.005.
Davies, G.F., 1992. On the emergence of plate-tectonics. Geology 20 (11), 963–966.
de Kock, M.O., Evans, D.A.D., Beukes, N.J., 2009. Validating the existence of Vaalbara in the Neoarchean. Precambrian Research 174, 145–154.
de Wit, M.J., 1998. On Archean granites, greenstones, cratons and tectonics: does the evidence demand a verdict? Precambrian Research 91 (1–2), 181–226.
Dhuime, B., Hawkesworth, C.J., Cawood, P.A., Storey, C.D., 2012. A change in the geodynamics of continental growth 3 billion years ago. Science 335, 1334–1336.
Djomani, Y.H.P., O'Reilly, S.Y., Griffin, W.L., Morgan, P., 2001. The density structure of subcontinental lithosphere through time. Earth and Planetary Science Letters 184, 605–621.
Dobmeier, C.J., Raith, M.M., 2003. Crustal architecture and evolution of the Eastern Ghats Belt and adjacent regions of India. In: Yoshida, M., Windley, B.F., Dasgupta, S. (Eds.), Proterozoic East Gondwana: Supercontinent Assembly and Breakup: Geological Society, London, Special Publication, 206, pp. 145–168.
Dobrzhinetskaya, L., Green, H.W., 2005. Ultra-deep subduction of continental crust: evidence from natural rocks and experimental investigations [abs.]. EOS. Transactions of the American Geophysical Union 86 (abstract V51E-01).
Domanik, K.J., Holloway, J.R., 2000. Experimental synthesis and phase relations of phengitic muscovite from 6.5 to 11 GPa in a calcareous metapelite from the Dabie Mountains, China. Lithos 52, 51–77.
Dumond, G., Mahan, K.H., Williams, M.L., Karlstrom, K.E., 2007. Crustal segmentation, composite looping pressure–temperature paths, and magma-enhanced metamorphic field gradients: Upper Granite Gorge, Grand Canyon, USA. Geological Society of America Bulletin 119, 202–220.
Duretz, T., Gerya, T.V., May, D.A., 2011. Numerical modelling of spontaneous slab breakoff and subsequent topographic response. Tectonophysics 502, 244–256.
Ehlers, C., Lindroos, A., Selonen, O., 1993. The late-Svecofennian granite–migmatite zone of southern Finland — a belt of transpressive deformation and granite emplacement. Precambrian Research 64, 295–309.
Elliott, T., Plank, T., Zindler, A., Wjite, W., Bourdon, B., 1997. Element transport from slab to volcanic front at the Mariana arc. Journal of Geophysical Research 102, 14991–15019.
Epard, J.L., Steck, A., 2008. Structural development of the Tso Morari ultra-high pressure nappe of the Ladakh Himalaya. Tectonophysics 451, 242–264.
Ernst, W.G., 2001. Subduction, ultrahigh-pressure metamorphism, and regurgitation of buoyant crustal slices — implications for arcs and continental growth. Physics of the Earth and Planetary Interiors 127, 253–275.
Evans, D.A.D., Mitchell, R.N., 2011. Assembly and breakup of the core of Paleoproterozoic–Mesoproterozoic supercontinent Nuna. Geology 443–446.
Faccenda, M., Gerya, T.V., Chakraborty, S., 2008. Styles of post-subduction collisional orogeny: influence of convergence velocity, crustal rheology and radiogenic heat production. Lithos 103, 257–287.
Faryad, S.W., Dobrzhinetskaya, L., Hoinkes, G., Zhang, J., 2013. Ultrahigh-pressure and high-pressure metamorphic terranes in orogenic belts: reactions, fluids and geological processes: preface. Gondwana Research 23, 841–843.
Faure, M., Lin, W., Scharer, U., Shu, L.S., Sun, Y., Arnaud, N., 2003. Continental subduction and exhumation of UHP rocks. Structural and geochronological insights from the Dabieshan (East China). Lithos 70, 213–241.
Galer, S.J.G., 1991. Interrelationships between continental freeboard, tectonics and mantle temperature. Earth and Planetary Science Letters 105, 214–228.
Gapais, D., Cagnard, F., Gueydan, F., Barbery, P., Ballevre, M., 2009. Mountain building and exhumation processes through time: inferences from nature and models. Terra Nova 21 (3), 188–194.
Gerya, T., 2014. Precambrian geodynamics: concepts and models. Gondwana Research 25, 442–463.
Gerya, T.V., Meilick, F.I., 2011. Geodynamic regimes of subduction under an active margin: effects of rheological weakening by fluids and melts. Journal of Metamorphic Geology 29, 7–31.
Gerya, T.V., Yuen, D.A., 2003. Characteristics-based marker-in-cell method with conservative finite-differences schemes for modeling geological flows with strongly variable transport properties. Physics of the Earth and Planetary Interiors 140, 295–318.
Goodwin, A.M., 1991. Precambrian Geology. Academic Press (666 pp.).
Gray, R., Pysklywec, R., 2010. Geodynamic models of Archean continental collision and the formation of mantle lithosphere keels. Geophysical Research Letters 37 (L19301). http://dx.doi.org/10.1029/2010GL043965 (5 pp.).
Gray, R., Pysklywec, R., 2012. Geodynamic models of mature continental collision: evolution of an orogen from lithospheric subduction to continental retreat/delamination. Journal of Geophysical Research 117, B03408. http://dx.doi.org/10.1029/2011JB008692.
Grove, T.L., Gaetani, G.A., de Wit, M.J., 1994. Spinifex textures in the 3.49 Ga Barberton mountain belt komatiites: evidence for crystalization of water-bearing cool magmas in the Archean. EOS. Transactions of the American Geophysical Union 75, 354.
Grove, T.L., Chatterjee, N., Parman, S.W., Medard, E., 2006. The influence of H_2O on mantle wedge melting. Earth and Planetary Science Letters 249, 74–89.

Gupta, S., 2012. Strain localization, granulite formation and geodynamic setting of 'hot orogens': a case study from the Eastern Ghats Province, India. Geological Journal 47, 334–351.
Hacker, B., Luffi, P., Lutkov, V., Minaev, V., Ratschbacher, L., Plank, T., Ducea, M., Patino-Douce, A., MvWillams, M., Matcalf, J., 2005. Near-ultrahigh pressure processing of continental crust: Miocene crustal xenoliths from the Pamir. Journal of Petrology 46, 1661–1687.
Hacker, B.R., Andersen, T.B., Johnston, S., Kylander-Clark, A.R.C., Peterman, E.M., Walsh, E.O., Young, D., 2010. High-temperature deformation during continental-margin subduction and exhumation: the ultrahigh-pressure Western Gneiss Region of Norway. Tectonophysics 480, 149–171.
Hamilton, W.B., 1998. Archean magmatism and deformation were not products of plate tectonics. Precambrian Research 91, 143–179.
Hamilton, W.B., 2011. Plate tectonics began in Neoproterozoic time, and plumes from deep mantle have never operated. Lithos 123, 1–20.
Hammer, P.T.C., Clowes, R.M., Cook, F.A., van der Velden, A.J., Vasudevan, K., 2010. The Lithoprobe trans-continental lithospheric cross sections: imaging the internal structure of the North American continent. Canadian Journal of Earth Sciences 47, 821–857.
Hawkesworth, C.J., Turner, S.P., McDermott, F., Peate, D.W., van Calsteren, P., 1997. U–Th isotopes in arc magmas: implications for element transfer from the subducted crust. Science 276, 551–555.
Herzberg, C., Asimow, P.D., Arndt, N., Niu, Y., Lesher, C.M., Fitton, J.G., Cheadle, M.J., Saunders, A.D., 2007. Temperatures in ambient mantle and plumes: constraints from basalts, picrites and komatiites. Geochemistry, Geophysics, Geosystems 8. http://dx.doi.org/10.1029/2006GC001390.
Herzberg, C., Condie, K., Korenaga, J., 2010. Thermal history of the Earth and its petrological expression. Earth and Planetary Science Letters 292, 79–88.
Irifune, T., Ringwood, A.E., Hibberson, W.O., 1994. Subduction of continental crust and terrigenous and pelagic sediments: an experimental study. Earth and Planetary Science Letters 126, 351–368.
Jahn, B., Caby, R., Monie, P., 2001. The oldest UHP eclogites of the world: age of UHP metamorphism, nature of protoliths, and tectonic implications. Chemical Geology 178, 143–158.
John, T., Scherer, E.E., Haase, K., Schenk, V., 2004. Trace element fractionation during fluid-induced eclogitization in a subducting slab: trace element and Lu–Hf–Sm–Nd isotope systematics. Earth and Planetary Science Letters 227, 441–456.
Kaneko, Y., Maruyama, S., Terabayashi, M., Yamamoto, H., Ishikawa, M., Anma, R., Parkinson, C.D., Ota, T., Nakajima, Y., Katayama, I., Yamamoto, J., Yamauchi, K., 2000. Geology of the Kokchetav UHP–HP metamorphic belt, Northern Kazakhstan. The Island Arc 9, 264–283.
Karlstrom, K.E., Williams, M.L., 2006. Nature of the middle crust-heterogeneity of structure and process due to pluton-enhanced tectonism: an example from Proterozoic rocks of the North American Southwest. In: Brown, M., Rushmer, T. (Eds.), Evolution and Differentiation of the Continental Crust. Cambridge University Press, Cambridge, pp. 268–295.
Keller, C.B., Schoene, B., 2012. Statistical geochemistry reveals disruption in secular lithospheric evolution about 2.5 Gyr ago. Nature 485, 490–493.
Korenaga, J., 2006. Archean geodynamics and thermal evolution of Earth. Archean geodynamics and environments. AGU Geophysical Monograph Series 164, 7–32.
Korhonen, F.J., Saw, A.K., Clark, C., Brown, M., Bhattacharya, S., 2011. New constraints on UHT metamorphism in the Eastern Ghats Province through the application of phase equilibria modelling and in situ geochronology. Gondwana Research 20, 764–781.
Korhonen, F.J., Clark, C., Brown, M., Bhattacharya, S., Taylor, R., in press. How long-lived is ultrahigh temperature (UHT) metamorphism? Constraints from zircon and monazite geochronology in the Eastern Ghats orogenic belt, India. Precambrian Research. http://dx.doi.org.proxy-um.researchport.umd.edu/10.1016/j.precamres.2012.12.001.
Korja, A., Heikkinen, P., 2005. The accretionary Svecofennian orogen — insight from the BABEL profiles. Precambrian Research 136, 241–268.
Korja, A., Lahtinen, R., Nironen, M., 2006. The Svecofennian orogen: a collage of microcontinents and island arcs. In: Gee, D.G., Stephenson, R.A. (Eds.), European Lithosphere Dynamics: Geological Society, London, Memoirs, 32, pp. 561–578.
Korsman, K., Hölttä, P., Hautala, T., Wasenius, P., 1984. Metamorphism as an indicator of evolution and structure of crust in eastern Finland. Bulletin — Geological Survey of Finland 328 (40 pp.).
Kukkonen, I.T., Lauri, L.S., 2009. Modelling the thermal evolution of a collisional Precambrian orogen: high heat production migmatitic granites of southern Finland. Precambrian Research 168, 233–246.
Kurhila, M., Vaasjoki, M., Mänttäri, I., Rämö, T., Nironen, M., 2005. U–Pb ages and Nd isotope characteristics of the lateorogenic, migmatizing microcline granites in southwestern Finland. Bulletin of the Geological Society of Finland 77, 105–128.
Kurhila, M., Andersen, T., Rämö, O.T., 2010. Diverse sources of crustal granitic magma: Lu–Hf isotope data on zircon in three Paleoproterozoic leucogranites of southern Finland. Lithos 115, 263–271.
Kurhila, M., Manttari, I., Vaasjoki, M., Ramo, O.T., Nironen, M., 2011. U–Pb geochronological constraints of the late Svecofennian leucogranites of southern Finland. Precambrian Research 190, 1–24.
Labrosse, S., Jaupart, C., 2007. Thermal evolution of the Earth: secular changes and fluctuations of plate characteristics. Earth and Planetary Science Letters 260, 465–481.
Lahtinen, R., Korja, A., Nironen, M., 2005. Paleoproterozoic tectonic evolution. In: Lehtinen, M., Nurmi, P.A., Rämö, O.T. (Eds.), Precambrian Geology of Finland—Key to the Evolution of the Fennoscandian Shield. Developments in Precambrian Geology, vol. 14. Elsevier B.V., Amsterdam, pp. 481–532.
Liou, J.G., Tsujimori, T., Zhang, R.Y., Katayama, I., Maruyama, S., 2004. Global UHP metamorphism and continental subduction/collision: the Himalayan model. International Geology Review 46, 1–27.
Little, T.A., Hacker, B.R., Gordon, S.M., Baldwin, S.L., Fitzgerald, P.G., Ellis, S., Korchinski, M., 2011. Diapiric exhumation of Earth's youngest (UHP) eclogites in the gneiss domes of the D'Entrecasteaux Islands, Papua New Guinea. Tectonophysics 510, 39–68.
Liu, L., Zhang, J., Green, H.W., Jin, Z., Bozhilov, K.N., 2007. Evidence of former stishovite in metamorphosed sediments, implying subduction to >350 km. Earth and Planetary Science Letters 263, 180–191.
Maierova, P., Lexa, O., Shulmann, K., Stipska, P., 2014. Contrasting tectono-metamorphic evolution of orogenic lower crust in the Bohemian Massif: a numerical model. Gondwana Research 25, 509–521.
Martin, H., Moyen, J.-F., Rapp, R., 2010. The sanukitoid series: magmatism at the Archaean–Proterozoic transition. Earth and Environmental Science Transactions of the Royal Society of Edinburgh 100 (Special Issue), 15–33.
McKenzie, D., Bickle, M., 1988. The volume and composition of melt generated by extension of the lithosphere. Journal of Petrology 29, 625–679.
Mishin, Y.A., Gerya, T.V., Burg, J.-P., Connolly, J.A.D., 2008. Dynamics of double subduction: numerical modeling. Physics of the Earth and Planetary Interiors 171, 280–295.
Moores, E.M., 2002. Pre-1 Ga (pre-Rodinian) ophiolites: their tectonic and environmental implications. Geological Society of America Bulletin 114, 80–95.
Mouri, H., Väisänen, M., Huhma, H., Korsman, K., 2005. Sm–Nd garnet and U–Pb monazite dating of high-grade metamorphism and crustal melting in the West Uusimaa area, southern Finland. GFF 127, 123–128.
Moyen, J.-F., van Hunen, J., 2011. Short-term episodicity of Archaean plate tectonics. Geology 40, 451–454.
Nie, S.M., Chiu, D.T., Zare, R.N., 1994. The exhumation of the Dabie–Shan ultra high-pressure rocks and accumulation of the Songpan–Ganzi flysch sequence, central China. Geology 22 (11), 999–1002.
Nikolaeva, K., Gerya, T.V., Connolly, J.A.D., 2008. Numerical modelling of crustal growth in intraoceanic volcanic arcs. Physics of the Earth and Planetary Interiors 171, 336–356.
Nisbet, E.G., Cheadle, M.J., Arndt, N.T., Bickle, M.J., 1993. Constraining the potential temperature of the Archean mantle: a review of the evidence from komatiites. Lithos 30, 291–307.
Okay, A., Sengör, A.M., 1992. Evidence for intracontinental thrust-related exhumation of the ultrahigh-pressure rocks in China. Geology 20, 411–414.
Okay, A., Sengör, A.M., Satir, M., 1993. Tectonics of an ultrahigh-pressure metamorphic terrane—the Dabie-Shan–Tongbai-shan orogen, China. Tectonics 12, 1320–1334.
Oueity, J., Clowes, R.M., 2010. Paleoproterozoic subduction in northwestern Canada from near-vertical and wide-angle seismic reflection data. Canadian Journal of Earth Sciences 47, 35–52.
Parman, S.W., Dann, J.C., Grove, T.L., de Wit, M.J., 1997. Emplacement conditions of komatiite magmas from the 3.49 Ga Komati Formation, Barberton greenstone belt, South Africa. Earth and Planetary Science Letters 150, 303–323.
Percival, J.A., Skulski, T., Sanborn-Barrie, M., Stott, G.M., Leclair, A.D., Corkery, M.T., Boily, M., 2012. Geology and tectonic evolution of the Superior Province, Canada, Chapter 6. In: Percival, J.A., Cook, F.A., Clowes, R.M. (Eds.), Tectonic Styles in Canada: The LITHOPROBE Perspective: Geological Association of Canada, Special Paper, 49, p. 512.
Ranalli, G., 1995. Rheology of the Earth. Chapman and Hall, London, p. 413.
Ratschbacher, L., Hacker, B.R., Webb, L.E., McWilliams, M., Ireland, T., Dong, S., Calvert, A., Chateigner, D., Wenk, H.R., 2000. Exhumation of the ultrahigh-pressure continental crust in east central China: Cretaceous and Cenozoic unroofing and the Tan–Lu fault. Journal of Geophysical Research — Solid Earth 105, 13303–13338.
Rey, P.F., Coltice, N., 2010. Neoarchean lithospheric strengthening and the coupling of Earth's geochemical reservoirs. Geology 36, 635–638.
Rey, P.F., Houseman, G., 2006. Lithospheric scale gravitational flow: the impact of body forces on orogenic processes from Archean to Phanerozoic. Analogue and Numerical modeling of crustal-scale processes, 253, pp. 153–167.
Rey, P.F., Philippot, P., Thébaud, N., 2003. Contribution of mantle plumes, crustal thickening and greenstone blanketing to the 2.75–2.65 Ga global crisis. Precambrian Research 127, 43–60.
Rickers, K., Mezger, K., Raith, M.M., 2001. Evolution of the continental crust in the Proterozoic Eastern Ghats Belt, and new constraints for Rodinia reconstruction: implications from Sm–Nd, Rb–Sr and Pb–Pb isotopes. Precambrian Research 112, 183–212.
Root, D.B., Hacker, B.R., Gans, P.B., Ducea, P.B., Eide, E.A., Mosenfelder, J.L., 2005. Discrete ultrahigh-pressure domains in the Western Gneiss Region, Norway: implications for formation and exhumation. Journal of Metamorphic Geology 23, 45–61.
Rutanen, H., Andersson, U.B., Väisänen, M., Johansson, A., Fröjdö, S., Lahaye, Y., Eklund, O., 2011. 1.8 Ga magmatism in southern Finland: strongly enriched mantle and juvenile crustal sources in a post-collisional setting. International Geology Review 53, 1622–1683.
Santosh, M., Sajeev, K., Li, J.H., Liu, S.J., Itaya, T., 2009. Counterclockwise exhumation of a hot orogen: the Paleoproterozoic ultrahigh-temperature granulites in the North China Craton. Lithos 110, 140–152.
Santosh, M., Liu, S.-J., Tsunogae, T., Li, J.-H., 2012. Paleoproterozoic ultrahigh-temperature granulites in the North China Craton: implications for tectonic models on extreme crustal metamorphism. Precambrian Research. http://dx.doi.org/10.1016/j.precamres.2011.05.003.
Schmeling, H., Babeyko, A.Y., Enns, A., Faccenna, C., Funiciello, F., Gerya, T., Golabek, G.J., Grigull, S., Kaus, B.J.P., Morra, G., Schmalholz, S.M., van Hunen, J., 2008. Benchmark comparison of spontaneous subduction models — towards a free surface. Physics of the Earth and Planetary Interiors 171 (1–4), 198–223.
Schmid, S.M., Kissling, E., 2000. The arc of the western Alps in the light of geophysical data on deep crustal structure. Tectonics 19 (1), 62–85.
Schmidt, M., Poli, S., 1998. Experimentally based water budgets for dehydrating slabs and consequences for arc magma generation. Earth and Planetary Science Letters 163, 361–379.

Searle, M., Hacker, B.R., Bilham, R., 2001. The Hindu Kush seismic zone as a paradigm for the creation of ultrahigh-pressure diamond- and coesite-bearing continental rocks. Journal of Geology 109, 143–153.

Sederholm, J.J., 1967. Selected Works: Granites and Migmatites.Oliver and Boyd, Edinburgh.

Sizova, E., Gerya, T., Brown, M., Perchuk, L.L., 2010. Subduction styles in the Precambrian: insight from numerical experiments. Lithos 116, 209–229.

Sizova, E., Gerya, T., Brown, M., 2012. Exhumation mechanisms of melt-bearing ultrahigh pressure crustal rocks during collision of spontaneously moving plates. Journal of Metamorphic Geology 30, 927–955.

Sleep, N.H., 2007. Plate tectonics through time. In: Stevenson, D. (Ed.), Treatise on 1258 Geophysics: Evolution of the Earth, vol. 9, pp. 145–169.

Smithies, R.H., van Kranendonk, M.J., Champion, D.C., 2007. The Mesoarchean emergence of modern-style subduction. Gondwana Research 11, 50–68.

Smithies, R.H., Howard, H.M., Evins, P.M., Kirkland, C.L., Kelsey, D.E., Hand, M., Wingate, M.T.D., Collins, A.S., Belousova, E., 2011. High-temperature granite magmatism, crust–mantle interaction and the Mesoproterozoic intracontinental evolution of the Musgrave Province, Central Australia. Journal of Petrology 52, 931–958.

Stern, R.J., 2005. Evidence from ophiolites, blueschists, and ultrahigh pressure metamorphic terranes that the modern episode of subduction tectonics begn in Neoproterozoic time. Geology 33, 557–560.

Toth, J., Gurnis, M., 1998. Dynamics of subduction initiation at preexisting fault zones. Journal of Geophysical Research — Solid Earth 103, 18053–18067.

Tsunogae, T., Liu, S.J., Santosh, M., Shimizu, H., Li, J.H., 2011. Ultrahigh-temperature metamorphism in Daqingshan, Inner Mongolia Suture Zone, North China Craton. Gondwana Research 20, 36–47.

Turcotte, D.L., Schubert, G., 2002. Geodynamics. Cambridge University Press, p. 456.

Väisänen, M., Mänttäri, I., Kriegsman, L.M., Hölttä, P., 2000. Tectonic setting of post-collisional magmatism in the Palaeoproterozoic Svecofennian orogen, SW Finland. Lithos 54, 63–81.

Väisänen, M., Mänttäri, I., Hölttä, P., 2002. Svecofennian magmatic and metamorphic evolution in southwestern Finland as revealed by U–Pb zircon SIMS geochronology. Precambrian Research 116, 111–127.

Valley, J.W., Lackey, J.S., Cavosie, A.J., Clechenko, C.C., Spicuzza, M.J., Basei, M.A.S., Bindeman, I.N., Ferreira, V.P., Sial, A.N., King, E.M., Peck, W.H., Sinha, A.K., Wei, C.S., 2005. 4.4 billion years of crustal maturation: oxygen isotope ratios of magmatic zircon. Contributions to Mineralogy and Petrology 150, 561–580.

van Hunen, J., Allen, M.B., 2011. Continental collision and slab break-off: a comparison of 3-D numerical models with observations. Earth and Planetary Science Letters 302, 27–37.

van Hunen, J., van den Berg, A.P., 2008. Plate tectonics on the early Earth: limitations imposed by strength and buoyancy of subducted lithosphere. Lithos 103 (1–2), 217–235.

Vogt, K., Gerya, T.V., 2014. From oceanic plateaus to allochthonous terranes: numerical modeling. Gondwana Research 25, 494–508.

Wallis, S., Tsuboi, M., Suzuki, K., Fanning, M., Jiang, L., Tanaka, T., 2005. Role of partial melting in the evolution of the Sulu (eastern China) ultrahigh-pressure terrane. Geology 33, 129–132.

Wang, Q.C., Cong, B.L., 1999. Exhumation of UHP terranes: a case study from the Dabie Mountains, eastern China. International Geology Review 41, 994–1004.

Wang, Q., Liu, X., Wu, W., 1997. Intrusive contact between granitic gneiss and UHP rocks: evidence from the Chinese Dabie Mountains and tectonic implications [abs.]. Fifth International Eclogite Conference. Terra Nova 9, 40.

Wu, Y., Fei, Y., Jin, Z., Liu, X., 2009. The fate of subducted Upper Continental Crust: an experimental study. Earth and Planetary Science Letters 282, 275–284.

Xu, Z., Zeng, L., Liu, F., Yang, J., Zhang, Z., McWilliams, M., Liou, J.G., 2006. Polyphase subduction and exhumation of the Sulu high-pressure–ultrahigh-pressure metamorphic terrane. Geological Society of America Special Papers 403, 93–113.

Yin, A., Nie, S.Y., 1993. Development of the Tan–Lu fault as a transform system collision of the north and south China blocks, east-central China. Tectonics 12, 801–813.

Yin, A., Manning, C.E., Lovera, O., Menold, C.A., Chen, X., Gehrels, G.E., 2007. Early Paleozoic tectonic and thermomechanical evolution of ultrahigh-pressure (UHP) metamorphic rocks in the Northern Tibetan plateau, Northwest China. International Geology Review 49, 681–716.